

Universiteit Utrecht

Condensed Matter & Interfaces

**Ion diffusion in lanthanide-doped
nanocrystals**

Ayla Dekker

Daily supervisor: Thomas van Swieten, MSc
Examined by: prof. dr. Andries Meijerink & dr. Freddy Rabouw



Universiteit Utrecht

16-12-2022

Abstract

The unique luminescence of lanthanide-doped nanocrystals has led to numerous scientific and technological applications. Over the last decades, synthesis methods have been developed to produce core/shell nanostructures, which enable spatial separation of dopant ions and thereby create new functionalities. Ionic diffusion is unwanted in these specific structures as it eliminates this spatial separation. On the other hand, the temperature dependence of ionic diffusion could also be useful, for instance to study migration of lanthanide ions under different conditions or to use in applications such as thermal history sensing. However, we currently lack the necessary practical, qualitative methods for measuring ion distribution. In this thesis, we study ion diffusion through simulations and experimental measurements. We calculated model decay curves from simulated concentration profiles to fit experimental decay curves from heated core/shell nanocrystals with different lanthanide dopants and shell lattices to study the effect of materials and temperature on diffusion speed. We found an increase by two orders of magnitude in the diffusion coefficient of $\text{NaYF}_4\text{:Ho}^{3+}/\text{NaYF}_4$ from $1.31 \cdot 10^{-24}$ to $1.11 \cdot 10^{-22}$ m^2/s when the temperature increased from 350 to 400 °C. Similar diffusion coefficients were found for $\text{NaYF}_4\text{:Ho}^{3+}/\text{NaGdF}_4$. Thus, we have successfully developed a modelling technique to enable facile and quantitative tracking of ion diffusion. This technique can help to gain insight to improve core/shell structures and develop thermal history sensors for independently measuring the temperature and duration of a heating event.

Contents

1	Introduction	3
2	Theoretical Background	5
2.1	Lanthanide luminescence	5
2.2	Decay dynamics	7
2.3	The shell model	8
2.4	Diffusion	9
3	Experimental	11
3.1	Synthesis	11
3.2	Luminescence measurements	13
4	Results and Discussion	14
4.1	Diffusion in NaYF ₄ nanocrystals	14
4.2	Diffusion model	21
4.3	Model fit to experimental data	24
5	Conclusion	28
6	Outlook	29
	Acknowledgements	30
	Bibliography	31
	Appendices	33

Chapter 1

Introduction

The luminescence of lanthanide-doped materials is becoming increasingly important for science and technology. Their remarkable optical properties have led to extensive use in various fields, such as lighting and displays.[1] Microcrystalline lanthanide-doped phosphors are for example frequently applied in white-light-emitting diodes[2][3][4] and anti-counterfeiting.[5][6] Recent advances in synthesis methods have extended the potential applications even further, by reducing crystal dimensions from the micrometre to nanometre scale.[7][8] These nanocrystals are highly useful as probes for bioimaging and single-molecule imaging.[9][10][11] New synthesis procedures and nanocrystal architectures are continuously developed to further enhance lanthanide-doped nanocrystals.

Currently, the design of nanocrystals is focused on core/shell architectures, which typically consist of a doped core enclosed in a shell that is either undoped or contains other dopant ions. In these structures, different dopant ions are spatially separated from each other or from molecules at the surface of the nanocrystal. Photon emission from lanthanide ions close to the crystal surface can be repressed by vibrations of nearby surface and solvent molecules,[12] an undoped shell creates spatial separation of the lanthanide ions and the surface, repressing the quenching of luminescence and thus increasing quantum yield as shown by Homann *et al.*[13] Doped shells are used to enable lanthanide pairings in a nanocrystal that might otherwise lead to quenching. For instance, Wang *et al.* showed that 808 nm light can be efficiently upconverted to 540 nm light by using nanocrystals with a erbium-and-ytterbium-doped core and a neodymium-and-ytterbium doped shell, where photons are absorbed by neodymium and emitted by erbium, facilitated by energy transfer via ytterbium. Without the core/shell induced spatial separation, neodymium ions would quench erbium emission.[14] The synthesis of core/shell particles with sharp interfaces between the core and the shell has proven to be difficult. Lanthanide migration between the core and the shell during synthesis has been observed on multiple occasions.[15][16][17] The intermixing of the lanthanide species eliminates the advantages of spatial separation. With an undoped shell, the migration brings the lanthanide ions back into proximity of the crystal surface. In both cases, the result is a reduced photon emission efficiency. Deeper understanding of ion diffusion is therefore important to better control the luminescence of lanthanide-doped materials.

Temperature is an important parameter that controls ion diffusion. The diffusion speed of an ion is described by its diffusion coefficient, which follows a Arrhenius-type dependence on the temperature.[18] Low (synthesis) temperatures therefore inhibit diffusion, which could be a solution to synthesise sharp core/shell interfaces. However, the temperature dependence of diffusion could also have interesting applications, as the extent of diffusion is a unique signature of the temperature that the material has been exposed to. This could be very useful in the field

of thermal history sensing. Currently, most thermal history sensors are based on a restructuring of the crystal lattice.[19] However, these processes are complex and a thorough understanding of the mechanism is still lacking. Diffusion on the other hand is a well-understood process that is extensively described in literature.[20][21][22] Current techniques to quantify ion diffusion rely on methods that are often impractical for actual application, such as the need for a particle accelerator.[23] There are simpler methods to study ion diffusion, such as luminescence, however they have only yielded qualitative information thus far.[15][16][24] A practical, quantitative technique to measure ion diffusion in solids would therefore be a useful addition to our understanding of diffusion.

In this thesis we develop a model to determine the diffusion coefficient from experimental luminescence decay measurements. First, we will provide theoretical background on lanthanide luminescence and ion diffusion in Chapter 2. In Chapter 3 our synthesis and measurement methods are described. The results we obtained from our luminescence decay measurements are described and discussed in Chapter 4. This chapter also contains an explanation of the model we constructed and its comparison to the experimental data. In Chapter 5 we draw conclusions from the obtained results and provide an outlook on further research and application.

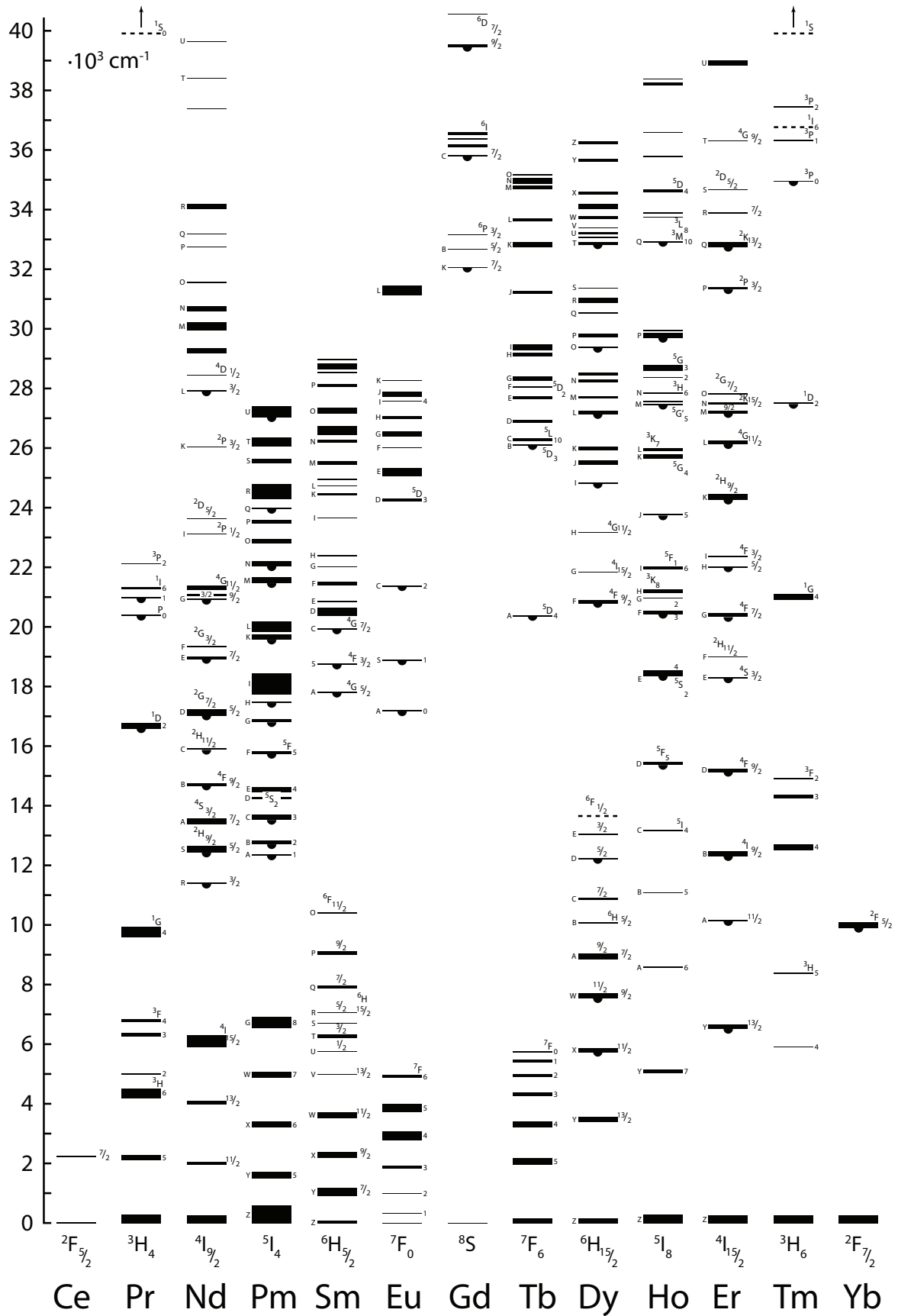


Figure 2.2: The Dieke diagram with the energy levels of the trivalent cationic lanthanides.

2.2 Decay dynamics

This rich energy level landscape gives rise to many possible electronic transitions. Starting from the lowest energy level, the ground level, a lanthanide can absorb a photon, exciting it to a higher-energy configuration as shown in Figure 2.3.a. This is a $4f^n \rightarrow 4f^n$ intra-configurational transition and thus creates no change in the electronic dipole moment.[27] Consequently, this transition is parity forbidden and the absorption is weak. Once the lanthanide occupies such an excited state, it can undergo multiple processes to return to a lower energy state.

We can describe this decay of the excited state in terms of decay rates. The change of excited state population over time is given by

$$\frac{dN}{dt} = -kN(t) \quad (2.1)$$

where $N(t)$ is the number of emitters in the excited state at a time t and k is the total decay rate of the excited state. The solution to this equation is

$$N(t) = N(0)e^{-kt} \quad (2.2)$$

with $N(0)$ the excited state population at $t = 0$. The excited ion can decay either radiatively or non-radiatively. Radiative decay is the emission of a photon by the ion (Figure 2.3.b). Depending on the photon energy, the emitter might relax to a lower lying excited state, or to the ground state. Similar to photon absorption, the emission of a photon is parity forbidden. Consequently, the radiative decay rates k_r of the f-f emissions are on the order of milliseconds.[28] Alternatively, an excited ion can decay non-radiatively. Multi-phonon relaxation is one of the main non-radiative decay mechanisms, it releases energy by emitting quanta of lattice vibrations known as phonons (Figure 2.3.c). The energy of a phonon depends on the crystal lattice, while the number of phonons depends on the size of the energy gap between the levels, making multi-phonon relaxation more likely for small gaps than for large gaps. The decay rates of both the radiative decay and the multi-phonon relaxation are independent of ion concentration, since these are both single ion processes.

Besides coupling of the excited state to photons and vibrations of the host lattice, lanthanide ions can also interact with other close-by ions. This interaction between ions is a form of Förster

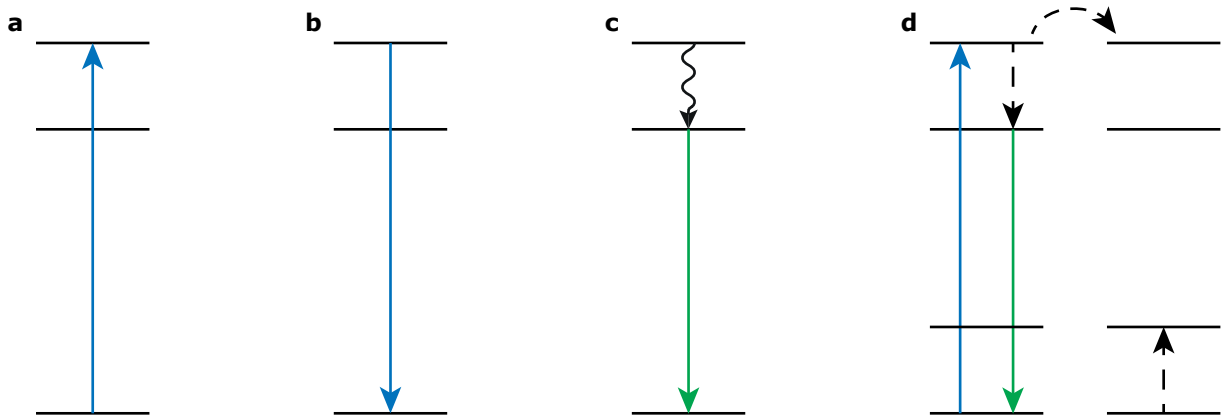


Figure 2.3: Schematic representation of a) excitation by absorption of a photon, b) luminescent decay by emission of a photon, c) multi-phonon relaxation followed by photon emission and d) cross-relaxation and subsequent photon emission.

energy transfer, making the decay rate of an electric-dipole–electric-dipole energy transfer k_{ET} proportional to the inverse sixth power of the distance between the ions:

$$k_{\text{ET}}(R) = \frac{C_X}{R^6} \quad (2.3)$$

where R is the distance between donor and acceptor and C_X a prefactor denoting the energy-transfer strength of a certain process which magnitude depends in part on the match between the energy difference of the levels in the donor and the acceptor. Although there are many different energy transfer mechanisms, we will focus on cross-relaxation as it is most relevant to this thesis. Cross-relaxation is the process in which part of the energy of the donor is transferred to an acceptor, both ions might then emit a photon or decay non-radiatively (2.3.d). As the rate of this process depends strongly on the distance between luminescent centres, cross-relaxation becomes more dominant at higher doping concentrations. Besides energy transfer to other ions and the host lattice (phonons), excited luminescent centres might also decay non-radiatively by energy transfer to ligands or surface defects. Due to the strong distance dependence and the relatively large surface area of small particles, the effect of this process becomes larger as the nanocrystals get smaller.

2.3 The shell model

To calculate the decay of the excited state population (Equation 2.2), the decay rates of every (prominent) decay process are needed. For single-ion processes such as radiative decay and multi-phonon relaxation, these rates are not dependent on concentration and can simply be determined from experimental decay curves. However, the energy transfer rate of cross-relaxation k_{ET} is not a constant, but depends strongly on the donor–acceptor distance (Equation 2.3). It is not possible to quantitatively calculate k_{ET} simply using the doping concentration, as the ions are not randomly placed with respect to one another, but built into a host lattice. Therefore, there are only some discrete ion-to-ion distances possible. To calculate these distances, we consider the crystal lattice of our host material. Figure 2.4 shows the crystal lattice of NaYF_4 in a two-dimensional projection. There are two different rare-earth positions, of which one is half occupied by sodium. From the rare-earth distribution in NaYF_4 and the doping concentration, we can calculate the cross-relaxation efficiency using the following expression:

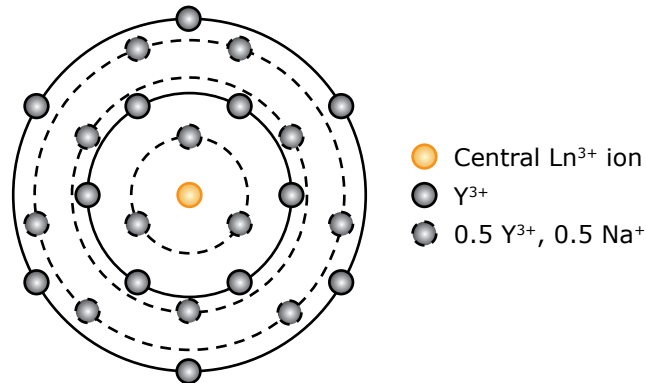


Figure 2.4: The two-dimensional representation of the NaYF_4 crystal lattice, adapted from Reference [29].

$$\begin{aligned}
X(C_X, \phi, t) = & \frac{2}{3} \prod_i \left(1 - \phi + \phi e^{-C_X t / R_i^6}\right)^{n_i} \times \prod_i \left(1 - \frac{\phi}{2} + \frac{\phi}{2} e^{-C_X t / R_i^{*6}}\right)^{n_i^*} \\
& + \frac{1}{3} \prod_i \left(1 - \frac{\phi}{2} + \frac{\phi}{2} e^{-C_X t / R_i^6}\right)^{n_i} \times \prod_i \left(1 - \phi + \phi e^{-C_X t / R_i^{*6}}\right)^{n_i^*}
\end{aligned} \tag{2.4}$$

where ϕ is the dopant concentration and C_X the cross-relaxation strength. The four terms stem from the complicated lattice structure of NaYF_4 . The summation over i would theoretically include the entire neighbour list, but practically one can cut off the summation at shells with a distance of around 2 nm, since the contribution of acceptors further away decreases rapidly due to the R^{-6} dependence. The contribution of multiple ions in the shell at distance R_i is added through the exponential n_i . The total decay of a luminescent centre is the product of the radiative, multi-phonon relaxation and cross-relaxation terms and therefore becomes

$$I(t) = X(C_X, \phi, t) e^{-kt} \tag{2.5}$$

in which k can be determined from decay measurements of materials with a low concentration of lanthanide ions, since the $X(C_X, \phi, t)$ term becomes negligible (Appendix 6.1.a). If k is known, $X(C_X, \phi, t)$ can then be determined from a series of decay curves from crystals with different dopant concentrations (Appendix 6.1.b). In this way, the decay curves can be calculated at all doping percentages for any material and energy level, even if their k and C_X values were not previously reported.

2.4 Diffusion

Around 1855 Adolf Fick conducted an extensive investigation on the diffusion of ions, specifically the diffusion of salt ions in water. His research was focussed on diffusion in liquids, as diffusion in solids was not believed to be possible at that time.[30] Later, when better equipment became available, diffusion in solids was studied and shown to behave similarly.[31]

Fick's work has led to two formulas, known simply as his first and second law. Fick's first law of diffusion describes the diffusive flux, the movement of particles from areas of high concentration to areas of low concentration. Its most common form in three dimensions is

$$J = -D \nabla \phi \tag{2.6}$$

where J is the diffusion flux vector, D the diffusion coefficient with dimension area per unit time (often m^2/s), ∇ the gradient operator and ϕ the concentration. The use of this law is limited, as it requires constant conditions over time. This formula does not apply if the flux of particles into and out of the system is not constant, which is why the second law was formulated.

Fick's second law of diffusion describes how the concentration gradient changes with respect to time,

$$\frac{\partial \phi}{\partial t} = D \Delta \phi \tag{2.7}$$

the gradient ∇ in the first law has been replaced by the Laplacian Δ , which is the second derivative with respect to space in three dimensions. For specific boundary conditions, such

as a delta function at $t = 0$ in an infinitely large space, there is an analytical solution, here $\phi = \frac{1}{\sqrt{4\pi Dt}} \exp\left(-\frac{x^2}{4Dt}\right)$ (one-dimension).[32] For more complex boundary conditions the concentration gradient as a function of time has to be calculated numerically.

The diffusion coefficient is constant for a combination of diffusing dopant species, diffusion host material and temperature. The temperature dependence of the diffusion coefficient can be described by

$$D(T) = D_0 \exp\left(-\frac{E_A}{k_B T}\right), \quad (2.8)$$

which is a variation of the Arrhenius equation. $D(T)$ is the diffusion coefficient used in Fick's laws of diffusion. D_0 is the diffusion coefficient at infinite temperature and thus the maximal D possible. E_A is the (material specific) activation energy for diffusion. k_B is the Boltzmann constant and T the temperature in kelvin.

Chapter 3

Experimental

3.1 Synthesis

3.1.1 Chemicals

All chemicals were used without further purification. The following chemicals were purchased from Aldrich: oleic acid (90 %, OA), terbium acetate hydrate (99.9 %, $\text{Tb}(\text{Ac})_3$), thulium acetate hydrate (99.9 %, $\text{Tm}(\text{Ac})_3$), yttrium acetate hydrate (99.9 %, $\text{Y}(\text{Ac})_3$) and gadolinium acetate hydrate (99.9 %, $\text{Gd}(\text{Ac})_3$). From Sigma-Aldrich, sodium hydroxide (>98 %, NaOH), ammonium fluoride (>98 %, NH_4F , stored in N_2 atmosphere) and 1-octadecene (90 %, ODE) were purchased. Holmium acetate hydrate (99.9 %, $\text{Ho}(\text{Ac})_3$) was purchased from Thermo scientific, ethanol (absolute, EtOH) from VWR, sodium oleate (>97 %, Na oleate) from TCI, n-hexane (hexane) from Alfa Aesar and cyclohexane (99.8 %, CH) was purchased from Acros organics.

3.1.2 Synthesis of Ln-doped NaYF_4 nanocrystals using Na oleate

The synthesis of core nanocrystals was carried out based on the method of Grauel *et al.*[33] using a Schlenk line setup. 7.5 mmol rare-earth acetates in the desired $\text{Y}(\text{Ac})_3/\text{Ho}(\text{Ac})_3$ (88:12), $\text{Y}(\text{Ac})_3/\text{Tb}(\text{Ac})_3$ (97:3) or $\text{Y}(\text{Ac})_3/\text{Tm}(\text{Ac})_3$ (95:5) ratio was added with 37.5 mmol Na oleate, 75 ml ODE and 75 ml OA to a 500 ml round-bottom flask. This was heated at 100 °C under vacuum for one hour and then evacuated three times, each time followed by a N_2 -flush. While maintaining a temperature of 100 °C, 60 mmol NH_4F was added under N_2 flow. This was flushed quickly three times by subjecting the flask to vacuum for 3–5 seconds before refilling with N_2 . After filling with N_2 , the mixture was heated to 310 °C (15 °C/min) and kept at this temperature for 55 minutes. After cooling to room temperature, 225 ml EtOH was added as anti-solvent and the suspension was centrifuged for 8 minutes at 2500 RPM (1222 RCF). The supernatant was discarded. The precipitate was re-dispersed in 20 ml hexane, 40 ml EtOH was added as anti-solvent and centrifuged for 8 minutes at 2500 RPM. After discarding the supernatant, the precipitate was re-dispersed in 20 ml hexane. The dispersion was centrifuged for 10 minutes at 2000 RPM (782 RCF) to remove by-products such as NaF. The supernatant was kept as core-nanocrystal dispersion.

3.1.3 Synthesis of Ln-doped NaYF_4 nanocrystals using NaOH

This synthesis of core nanocrystals was done in a Schlenk line based on the work of Geitenbeek *et al.*[34] First, 4 mmol $\text{Ln}(\text{Ac})_3$ was combined in the required ratio with 24 ml OA and 68 ml ODE in a 250 ml round-bottom flask. This was degassed under vacuum at 120 °C for

90 minutes. Then, the mixture was flushed three times with vacuum and N_2 and cooled to room temperature. 12 mmol NaOH and 16 mmol NH_4F were dissolved in 10 ml and 30 ml EtOH, respectively. The Na and F precursors were mixed and quickly added to the rare-earth solution. The resulting mixture was stirred for 16 hours. Afterwards, the methanol was removed by heating to 100 °C under vacuum, followed by 30 minutes of degassing and subsequent flushing with N_2 and vacuum three times. The reaction mixture was heated to 300 °C under N_2 atmosphere (15 °C/min) for 110 minutes. After cooling to room temperature, 90 ml EtOH was added and the mixture was centrifuged at 2500 RPM for 8 minutes. The supernatant was discarded and the precipitate was washed twice by re-dispersion in 40 ml hexane, adding 40 ml ethanol as anti-solvent and centrifuging for 8 minutes at 2500 RPM. The resulting precipitate was dispersed in 15 ml CH. As dissolved NaOH is used in this procedure, OH^- ions might be incorporated in the crystal lattice during synthesis. Since this might affect the diffusion or decay rates of the lanthanide dopants, we used the procedure in Section 3.1.2 for most nanocrystals.

3.1.4 Synthesis of the shell precursor

Based on the method of Homann *et al.*,[13] a shell-material precursor was made. First, 150 ml ODE and 150 ml OA were degassed together in a 500 ml flask in a Schlenk line under vacuum at 80 °C for 1 hour. 13.5 mmol $Ln(Ac)_3$ ($Ln = Y$ or Gd) was added under N_2 flow. The mixture was heated to 100 °C for 60 minutes under vacuum. 20 mmol Na oleate was added under N_2 flow, the mixture was evacuated three times, each time followed by a N_2 -flush. 55 mmol NH_4F was added under N_2 flow, afterwards flushing three times quickly by submitting the flask to vacuum for 3–5 seconds before refilling with N_2 . The reaction mixture was heated to 200 °C (15 °C/min) and kept at this temperature for 1 hour. After cooling to room temperature, the reaction mixture was centrifuged for 10 minutes at 3000 RPM (1760 RCF). The precipitate was discarded. 450 ml EtOH was added to the supernatant, which was then centrifuged for 10 minutes at 3000 RPM. The supernatant was discarded. The precipitate was washed twice by re-dispersing in 60 ml hexane, adding 110 ml EtOH as anti-solvent, then centrifuging for 10 minutes at 3000 RPM. The resulting precipitate was re-dispersed in 15 ml hexane.

3.1.5 Shell growth

To grow the shell around the cores, our procedure was based on the method described by Homann *et al.*,[13] First, the weight concentrations of nanocrystals in the core and shell-precursor dispersions were determined. Then, 0.125 mmol core material (assuming a 33% molecular weight increase due to organic ligands) and 0.875 mmol shell material (assuming 100% molecular weight increase from ligands) were added to a 50 ml flask with 4 ml ODE and 4 ml OA. The hexane from the dispersions is removed by heating to 100 °C under vacuum at which the mixture was degassed for 1 hour and flushed 3 times with vacuum and N_2 . The mixture was heated to 300 °C (20 °C/min) and kept at this temperature for 2 hours. The reaction mixture was cooled to room temperature. Then 12 ml EtOH was added as anti-solvent and centrifuged for 8 minutes at 2500 RPM. The supernatant was discarded. The precipitate was washed twice by re-dispersion in 5 ml hexane, addition of 5 ml EtOH, then centrifuging for 8 minutes at 2500 RPM. The resulting precipitate was dispersed in 10 ml CH. When taking aliquots over time (Appendix 6.2), the scale of the synthesis was doubled. The 0.5 millilitre aliquots were extracted from the reaction through a septum using a syringe and immediately added to 0.5 ml EtOH. Washing was similar to the main product.

3.2 Luminescence measurements

Emission spectra and luminescence decay curves were measured using an Ekspla NT342B OPO laser (10 Hz), a Triax 550 monochromator, and a Hamamatsu R928 PMT (emission spectra) or Hamamatsu H7422 PMT (decay curves). An OBIS laser (1 mW, 25 Hz) was used for excitation at 374 nm. The heating of samples was done using a Linkam THMS600 microscope stage. The decay curves of Appendix 6.2 were measured using a large sample holder (Figure 3.1.a). However, we found that heating in this holder was not homogeneous across the sample, so all other measurements and heating were done using a smaller sample holder (Figure 3.1.b).

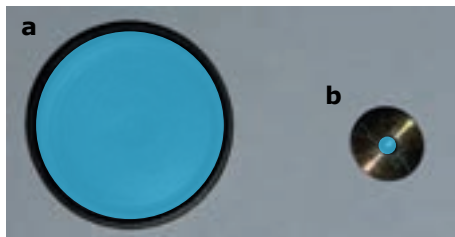


Figure 3.1: The a) large and b) small sample holders used for measurements. The blue circles indicate the placement of sample material.

Chapter 4

Results and Discussion

4.1 Diffusion in NaYF₄ nanocrystals

To study the diffusion of lanthanide ions in nanocrystals (NCs), we made doped-core-undoped-shell NCs and compared the decay curves before and after heating. As we want to know the influence of host material and dopant species on ion diffusion, we used two different kinds of shell material (NaYF₄ and NaGdF₄) and three different lanthanide dopants (holmium, terbium, and thulium).

4.1.1 NaYF₄:Ho³⁺

Figure 4.1.a shows the TEM image of NaYF₄:Ho³⁺(12%) NCs (Section 3.1.2) with 3.2 ± 0.1 nm radius, this small standard deviation indicates monodisperse particles. NaYF₄ and NaGdF₄ shells were grown around these cores, separately (Section 3.1.5). The NaYF₄:Ho³⁺/NaYF₄ NCs are 7.6 ± 0.3 nm in size (Figure 4.1.b) and the NaYF₄:Ho³⁺/NaGdF₄ NCs 8.2 ± 0.6 nm (Figure 4.1.c), resulting in a shell thickness of 4.4 and 5.0 nm, respectively.

In Figure 4.2 we show the decay curves of the green ⁵S₂ emission upon resonant excitation of the core-only and the core/shell NCs without any heating. We observe slower decay from the core/shell NCs than from the core-only particles. This is an unexpected observation because the shell material does not contain lanthanide dopants and would therefore not be expected to influence the decay curve. One possible explanation is the reduction of surface quenching by

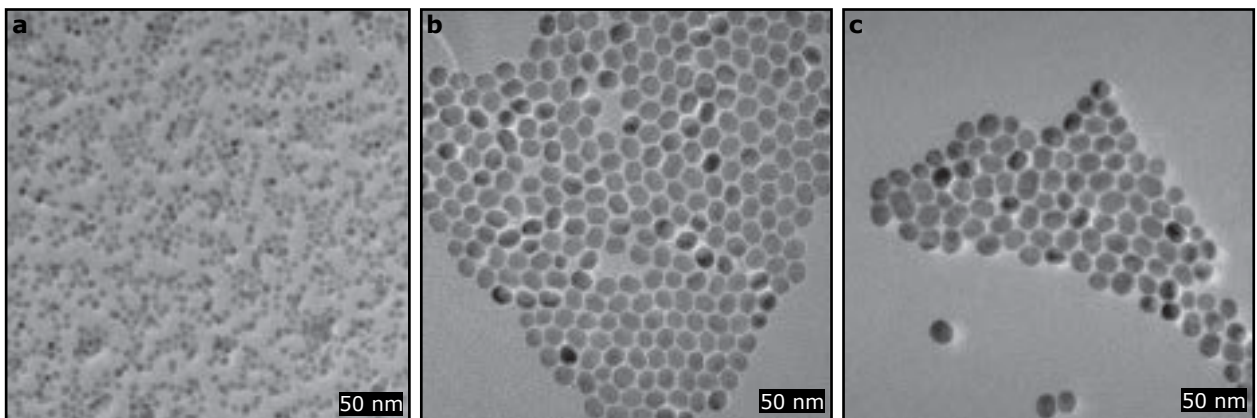


Figure 4.1: TEM images of (a) NaYF₄:Ho³⁺(12%) core NCs with a radius of 3.2 ± 0.1 nm, (b) NaYF₄:Ho³⁺(12%)/NaYF₄ core/shell NCs with a radius of 7.6 ± 0.3 nm, and (c) NaYF₄:Ho³⁺(12%)/NaGdF₄ core/shell NCs with a radius of 8.2 ± 0.6 nm.

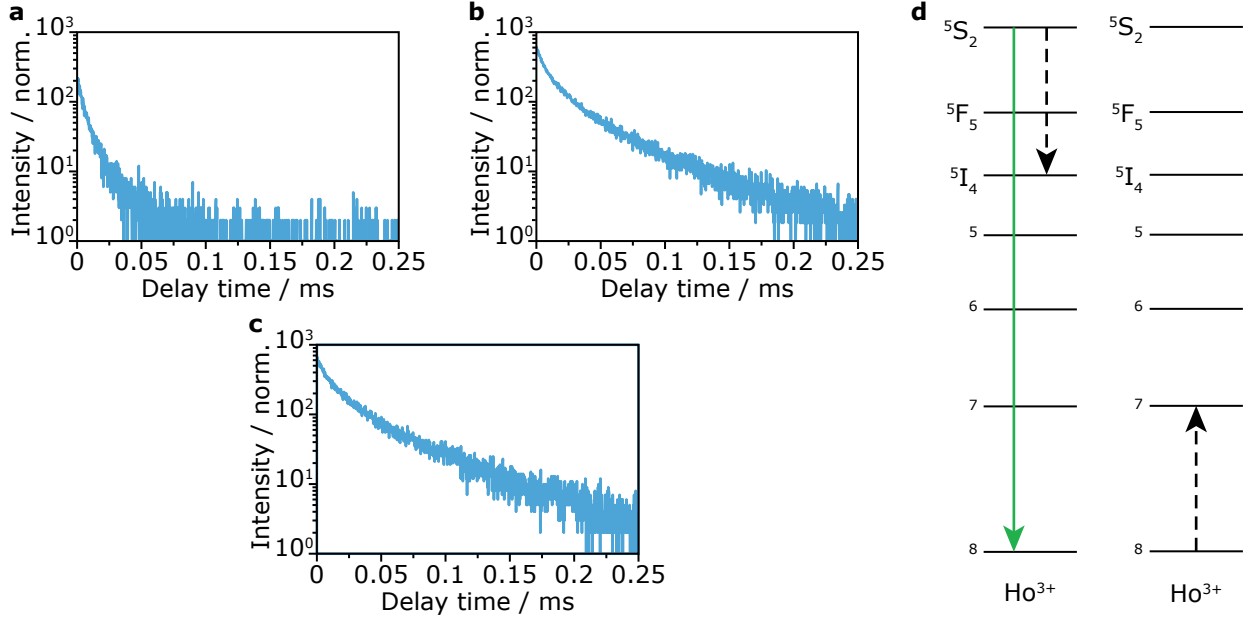


Figure 4.2: Luminescence decay curves of the 5S_2 emission of a) NaYF₄:Ho³⁺ (12%), b) NaYF₄:Ho³⁺ (12%)/NaYF₄, c) NaYF₄:Ho³⁺ (12%)/NaGdF₄. Excitation and emission wavelengths were 532 nm and 551 nm, respectively. d) The simplified energy level diagram of holmium showing the green (551 nm) emission used in decay measurements of the 5S_2 level. The dashed arrows show the cross-relaxation process.

the shell. As the shell puts distance between the lanthanide ions and the surface, there are no ions near the surface that can decay by coupling to surface defects and vibrations in the ligands (Section 2.2).[13] However, this surface quenching only contributes to the decay at very short delay times, because the energy transfer at the surface is really fast. Since we observe slower decay at longer delay times, we cannot attribute this observation to surface quenching. A more likely explanation is the diffusion of holmium ions already during shell growth (Appendix 6.2), as this is also seen in literature.[35][36][37] The elevated temperature of the synthesis (Section 3.1.5) makes diffusion of the ions significant. Alternatively or additionally, the outer crystal structure of the cores is slightly restructured with the addition of shell material, causing intermixing of the two lattices as opposed to a sharp interface.

We analyse further diffusion of holmium at elevated temperature by heating the NaYF₄:Ho³⁺/NaYF₄ NCs to 350 °C. Figure 4.3.a shows the luminescence decay curves of the 5S_2 emission of the core-only NCs (purple), the core/shell NCs before heating (dark blue), and the core/shell NCs heated at 350 °C for 10, 20, 30, and 60 minutes (light blue, green, yellow, and orange, respectively). We also heated the core/shell NCs to 550 °C for 30 minutes (red curve) as a comparison to the other measurements as a homogeneous distribution of ions has been reached under these conditions. After 10 minutes of heating, we see a slower decay at long delay times, compared to the unheated NCs. This trend continues with increasing heating durations. As lower holmium concentrations result in slower decay rates, this trend seems to indicate more extensive diffusion for longer heating times. The diffusing ions likely come from the edge of the core, not the centre, since the decay curve at short delay times is dominated by the highly concentrated ions in the core and we only see a small change at the start of the curve. The slowly decaying tail of the curve is caused by the diffused ions in the shell, where there is a very low holmium concentration. The decay curve after 60 minutes shows faster decay than after heating at 550

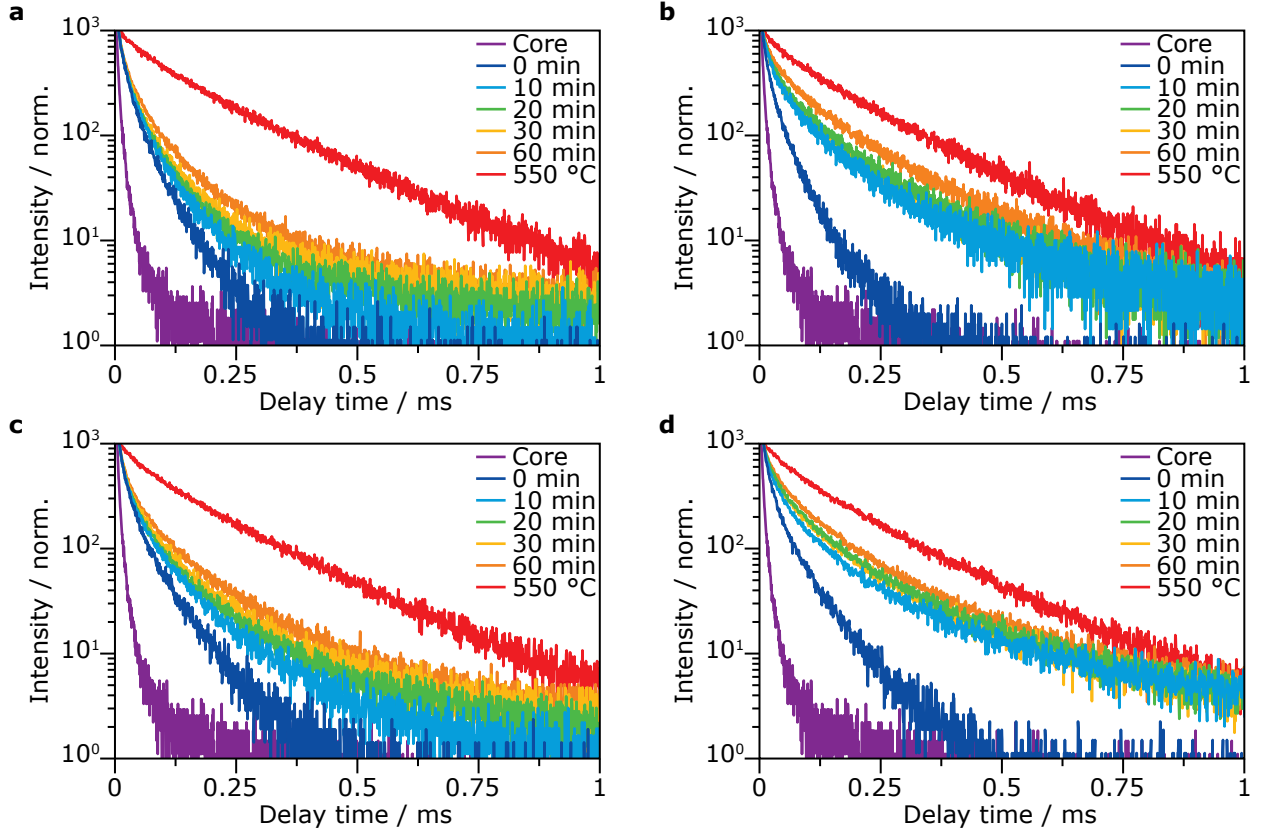


Figure 4.3: Luminescence decay curves of the 5S_2 emission of Ho^{3+} , measured after various heating steps. (a) Decay curves of $\text{NaYF}_4:\text{Ho}^{3+}/\text{NaYF}_4$ heated at $350\text{ }^\circ\text{C}$. (b) Same as in (a) but heated at $400\text{ }^\circ\text{C}$. (c-d) Same as in (a-b) but for $\text{NaYF}_4:\text{Ho}^{3+}/\text{NaGdF}_4$. Heating times are given in the legends. The purple curve gives the decay of the unheated core NCs and the dark blue curves correspond to the respective unheated core/shell NCs. The red curves were obtained by heating the 60 minute samples for an additional 30 minutes at $550\text{ }^\circ\text{C}$. Excitation and emission wavelengths were 532 nm and 551 nm , respectively.

$^\circ\text{C}$, suggesting further diffusion is still possible after heating at $350\text{ }^\circ\text{C}$ for 60 minutes. So, there is significant diffusion after heating at $350\text{ }^\circ\text{C}$, but to reach homogenous ion distribution either the temperature has to be increased or the heating time needs to be extended to well over an hour.

To study the effect of temperature on the lanthanide diffusion, we perform the same set of experiments in Figure 4.3.b as in 4.3.a, but heated at $400\text{ }^\circ\text{C}$ instead of $350\text{ }^\circ\text{C}$. Similarly, we see a trend of slower decay with increasing heating time. Unlike heating at $350\text{ }^\circ\text{C}$, we see a significant decrease in decay rate at short delay times when heated at $400\text{ }^\circ\text{C}$. This fast decay at short delay times is caused by the highly concentrated ions in the centre of the core. A lower concentration in the core, would result in slower decay at short delay times. Therefore, this result suggests faster diffusion for higher heating temperatures, as more ions have diffused from the core to the shell within 60 minutes for heating at $400\text{ }^\circ\text{C}$ than at $350\text{ }^\circ\text{C}$. This is in accordance with our expectation based on theory (Section 2.4).

Besides the temperature-dependence of ion diffusion, we are also interested in the impact of the host lattice on ion diffusion, to this end we repeated this experimental work on $\text{NaYF}_4:\text{Ho}^{3+}/\text{NaGdF}_4$ NCs (Figure 4.3.c/d). Similar to the results on $\text{NaYF}_4:\text{Ho}^{3+}/\text{NaYF}_4$, we see a trend of slower decay with longer heating and slower decay rates for heating at 400

°C than at 350 °C. Therefore we can draw the same conclusions that the holmium ions diffuse further at longer heating times and diffusion is faster at higher heating temperatures. Since it is difficult to distinguish differences between panels a) and c), or between panels b) and d) by eye, a quantitative model is required to further analyse the effect of the host lattice on ion diffusion, which we implement in Section 4.3.

4.1.2 NaYF₄:Tb³⁺

To acquire a better understanding of how the dopant size and weight influence diffusion, we performed a similar set of experiments using Tb³⁺ as the dopant ion. The radius of Tb³⁺ is 0.023 Å larger than Ho³⁺, while its mass is 6 u lower.[38] It is difficult to predict whether terbium will diffuse faster or slower than holmium, as we expect slower diffusion for a larger ion, but faster diffusion for lighter ions.

The terbium-doped NCs are shown in Figure 4.4 using TEM images. The NCs are monodisperse and have a radius of 4.0 ± 0.2 nm (NaYF₄:Tb³⁺(3%)), 8.2 ± 0.3 nm (NaYF₄:Tb³⁺/NaYF₄), and 8.4 ± 0.5 nm (NaYF₄:Tb³⁺/NaGdF₄). Figure 4.5 shows the decay curves measured from the ⁵D₃ terbium level. Similar to the results of the Ho³⁺-doped NCs, we observe slower decay at longer heating times and faster decay of the core-only particles than the core/shell NCs. The main difference between the Ho³⁺- and Tb³⁺-doped NCs is the slower decay of the unheated terbium core/shell NCs compared to the heated samples. This is most clearly visible in Figure 4.5.a, where the decay becomes increasingly slower for longer heating times, but is still faster after 60 minutes of heating at 350 °C than the decay of the unheated particles. This is an expected observation as heating induces diffusion and the diffusion of ions leads to slower decay. Possibly, the high temperature causes the NCs to coalesce, influencing their luminescence decay.[34]

To find an explanation for the unexpected trend in Figure 4.5, we measured the steady-state luminescence of NaYF₄:Tb³⁺/NaGdF₄ NCs before and after heating at 350 °C to study the influence of heating on the ratio between emission from the ⁵D₄ and ⁵D₃ levels. As a result of diffusion we expect the ion concentration to be lower after heating, resulting in less efficient cross-relaxation and thus less feeding from the ⁵D₃ to the ⁵D₄ level, which should in turn de-

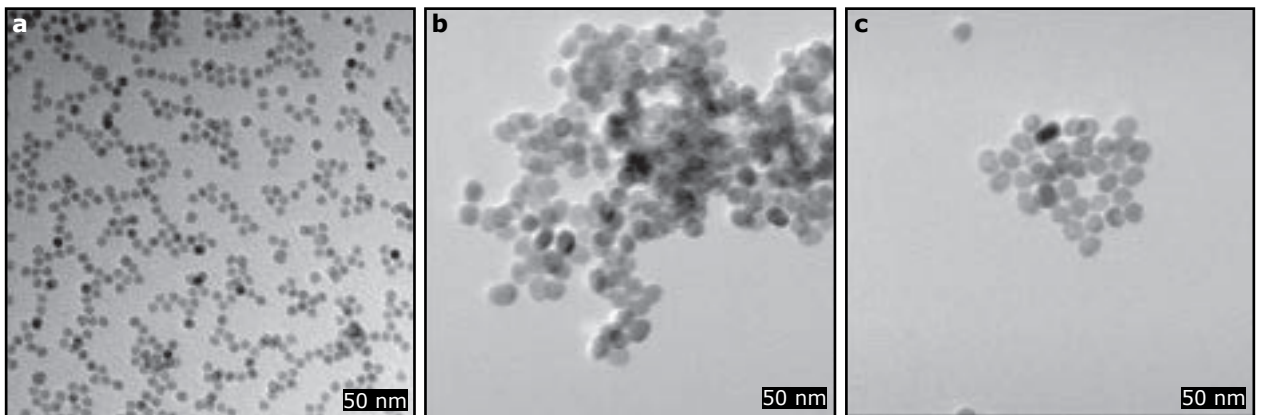


Figure 4.4: TEM images of (a) NaYF₄:Tb³⁺(3%) core NCs with a radius of 4.0 ± 0.2 nm, (b) NaYF₄:Tb³⁺(3%)/NaYF₄ core/shell NCs with a radius of 8.2 ± 0.3 nm, and (c) NaYF₄:Tb³⁺(3%)/NaGdF₄ core/shell NCs with a radius of 8.4 ± 0.5 nm.

crease the ${}^5D_4/{}^5D_3$ emission ratio. A deviation in this expected trend or additional features in the emission spectra might give an indication of the cause of the trend in Figure 4.5. The spectra showed a high level of non-Tb $^{3+}$ -related background (Figure 4.6.b), likely due to fluorescence of organic contaminants, making direct comparison between the luminescence before and after heating challenging. We therefore measured decay curves from the 5D_4 level under the same heating conditions as measurements on the 5D_3 level (Figure 4.6.c), which makes it possible to determine the ratio from the integral of the Tb $^{3+}$ decay curves. The decay of the unheated NCs is as expected. We see a rise at short delay times as this level is fed by cross relaxation from 5D_3 (Figure 4.6.a), followed by slow, mono-exponential decay. After heating, the rise is no longer visible, likely due to a dominating, fast decay at short delay times. In addition, the decay curves are multi-exponential after heating. This trend is puzzling, since multi-exponential decay is seen for the donor in a cross-relaxation pair, not for an acceptor like the 5D_4 level (Section 2.3). By taking the integral under each decay curve, we calculated the emission ratios between the 5D_4 and 5D_3 level (Figure 4.6.d). We did not find the expected decreasing 5D_4 to 5D_3 ratio with heating time, instead the ratios first increase and are significantly higher for NCs heated up to an hour than for the unheated NCs. Clearly, the luminescence of these Tb $^{3+}$ -doped samples is not suited to study ion diffusion.

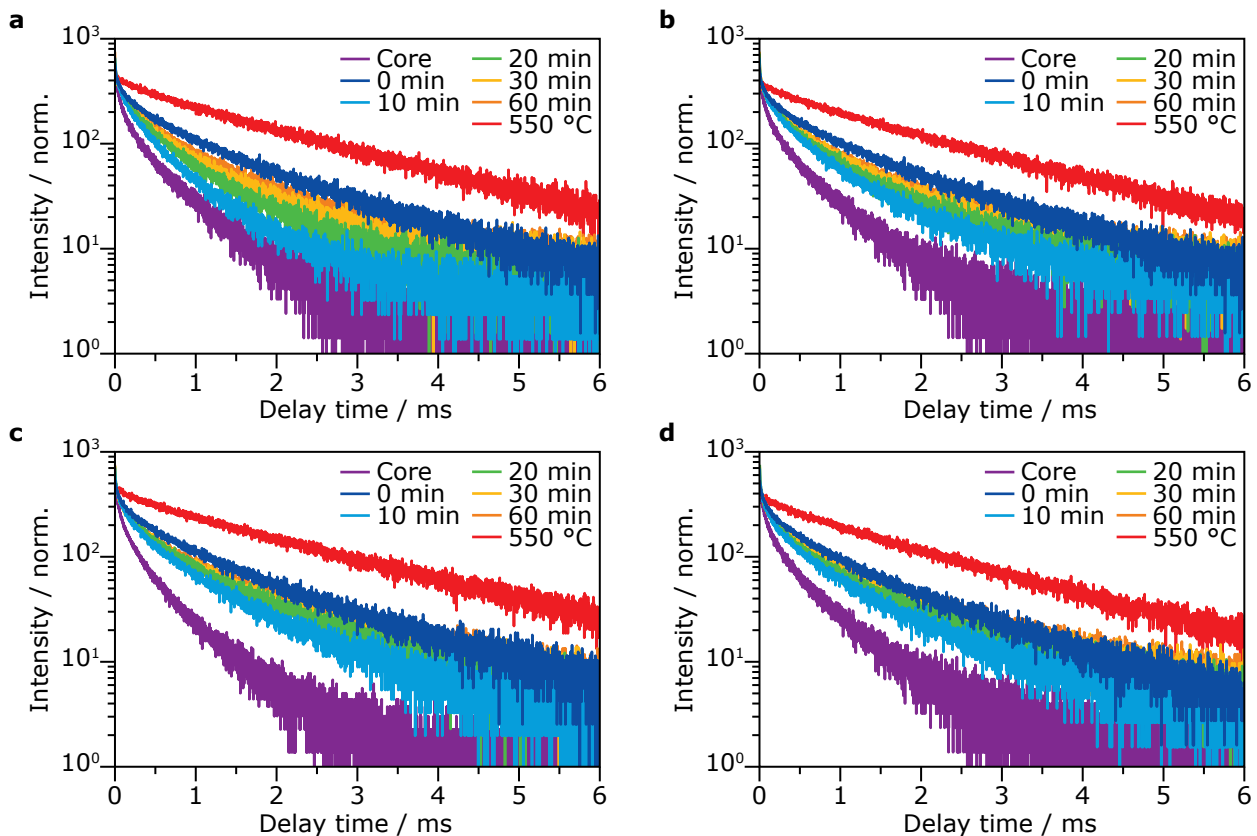


Figure 4.5: Luminescence decay curves of 5D_3 emission of a) NaYF $_4$:Tb $^{3+}$ (3%)/NaYF $_4$ NCs heated at 350 °C, b) NaYF $_4$:Tb $^{3+}$ (3%)/NaYF $_4$ NCs heated at 400 °C, c) NaYF $_4$:Tb $^{3+}$ (3%)/NaGdF $_4$ NCs heated at 350 °C, and d) NaYF $_4$:Tb $^{3+}$ (3%)/NaGdF $_4$ NCs heated at 400 °C. Heating times are given in the legends. The purple curve gives the decay of the unheated core NCs and the dark blue curves correspond to the respective unheated core/shell NCs. The red curves were obtained by heating the 60 minute samples for an additional 30 minutes at 550 °C. Excitation and emission wavelengths were 380 nm and 410 nm, respectively.

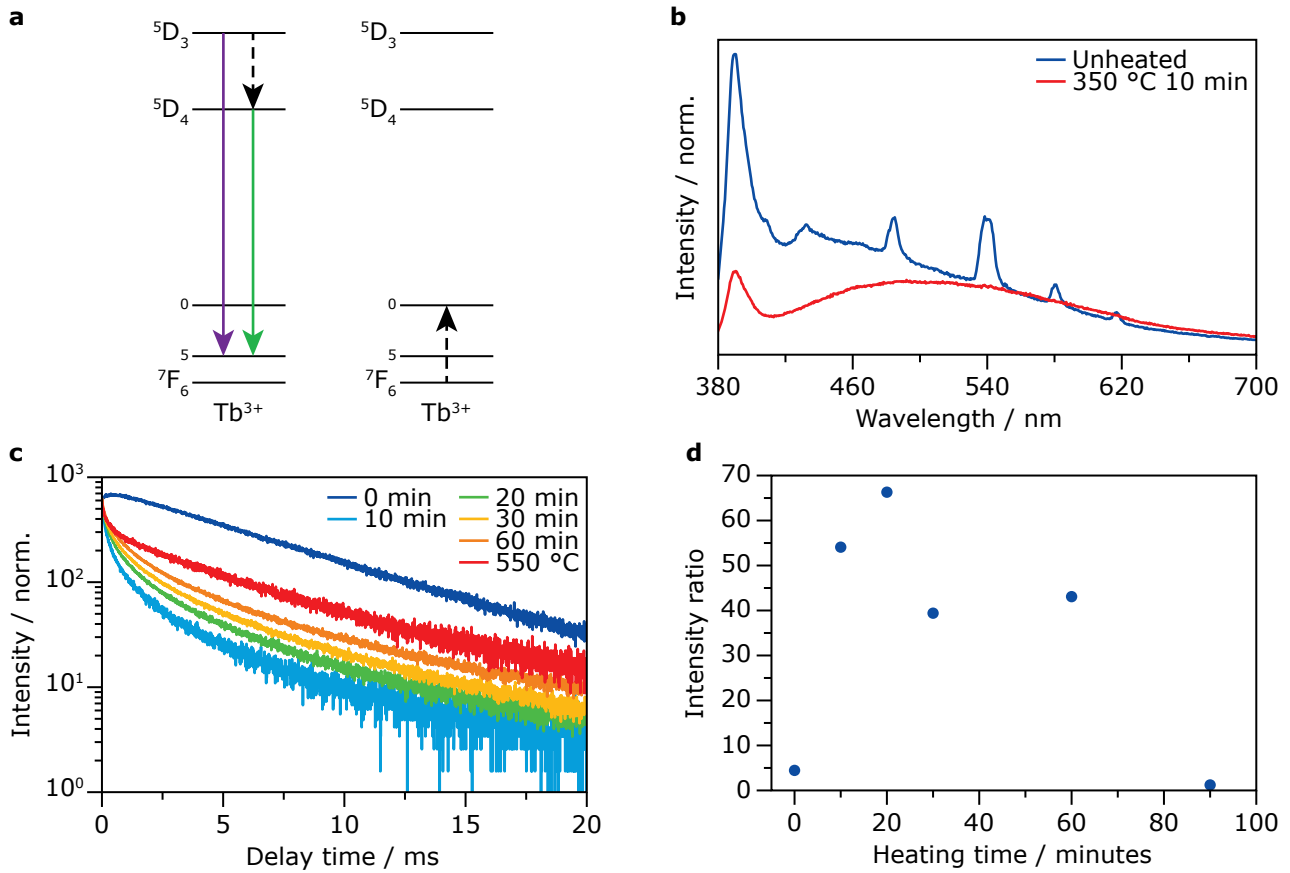


Figure 4.6: a) The simplified energy level diagram of terbium showing the violet (410 nm) and green (543 nm) emission measured for 5D_3 and 5D_4 decay measurements, respectively. The dashed arrows show the cross-relaxation process. b) Emission spectra of $\text{NaYF}_4:\text{Tb}^{3+}(3\%)/\text{NaGdF}_4$ NCs unheated and heated at 350 °C for 10 minutes, excited with a 374 nm laser. c) 5D_4 Decay curves of $\text{NaYF}_4:\text{Tb}^{3+}(3\%)/\text{NaGdF}_4$ NCs heated at 350 °C. The dark blue curve corresponds to the unheated core/shell NCs. The red curve was obtained by heating the 60 minute samples for an additional 30 minutes at 550 °C. Excitation and emission wavelengths were 374 nm and 543 nm, respectively. d) The $^5D_4/5D_3$ emission ratio as determined from the integral under the decay curves measured after heating at 350 °C, except for the 90 minute measurement, these NCs were heated at 350 °C for 60 minutes and 550 °C for 30 minutes.

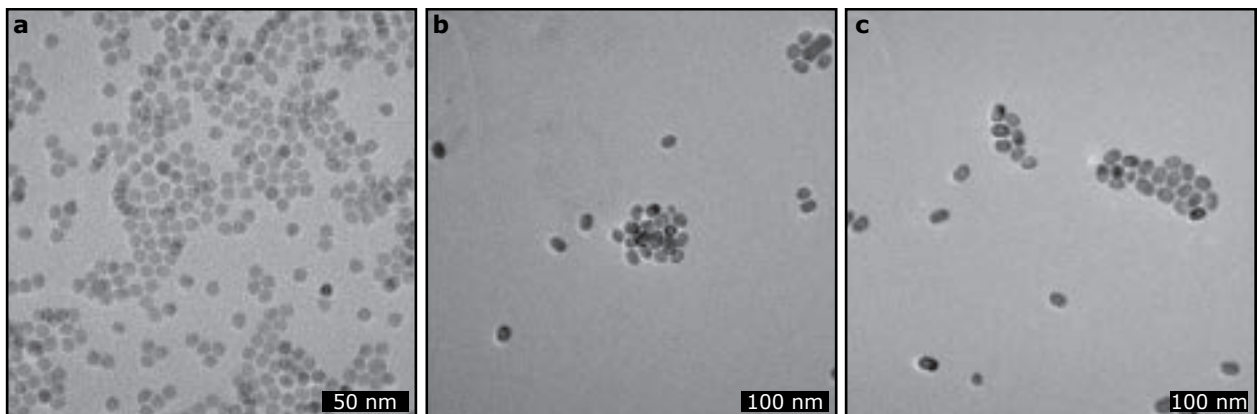


Figure 4.7: TEM images of (a) $\text{NaYF}_4:\text{Tm}^{3+}(5\%)$ core NCs with a radius of 4.1 ± 0.1 nm, (b) $\text{NaYF}_4:\text{Tm}^{3+}(5\%)/\text{NaYF}_4$ core/shell NCs with a radius of 9.5 ± 0.7 nm, and (c) $\text{NaYF}_4:\text{Tm}^{3+}(5\%)/\text{NaGdF}_4$ core/shell NCs with a radius of 10.4 ± 3.2 nm.

4.1.3 NaYF₄:Tm³⁺

From TEM images (Figure 4.7) we find the NaYF₄:Tm³⁺(5%), NaYF₄:Tm³⁺(5%)/NaYF₄, and NaYF₄:Tm³⁺(5%)/NaGdF₄ NC radii to be 4.1 ± 0.1 nm, 9.5 ± 0.7 nm, and 10.4 ± 3.2 nm, respectively. As can be seen in Figure 4.8, the core-only NCs have a slower ¹G₄ decay at short delay times than even the core/shell NCs with the longest heating times. This is unexpected, since the core NCs have the highest thulium concentration, which leads to the most efficient cross-relaxation and thus fastest decay. Similarly, we expect heated core/shell NCs to have slower decay than the unheated NCs, as diffusing ions would lower the core concentration, but we observe the opposite trend. Furthermore does the luminescence decay change only weakly with increasing heating times with no particular trend.

To further study the decay from thulium, we measured the decay curves of core-only NCs unheated and heated for 30 minutes at 350 °C (Figure 4.9.a). The decay should be the same before and after heating as there is no diffusion in core-only particles, however we clearly see

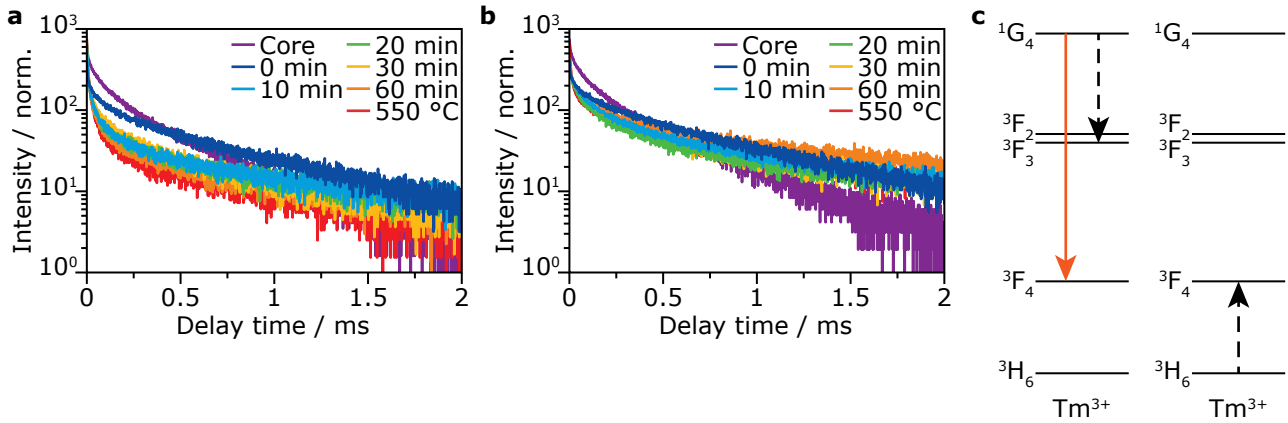


Figure 4.8: ¹G₄ Decay curves of a) NaYF₄:Tm³⁺(5%)/NaYF₄ and b) NaYF₄:Tm³⁺(5%)/NaGdF₄ NCs heated at 450 °C. Heating times are given in the legends. The purple curve gives the decay of the unheated core NCs and the dark blue curves correspond to the respective unheated core/shell NCs. The red curves were obtained by heating the 60 minute samples for an additional 30 minutes at 550 °C. Excitation and emission wavelengths were 471 nm and 642 nm, respectively.

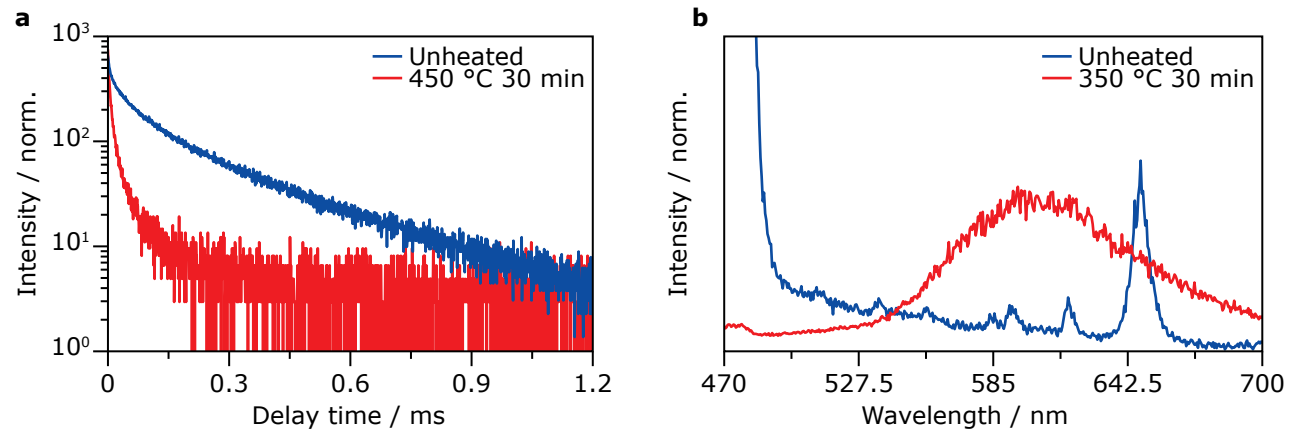


Figure 4.9: ¹G₄ Decay curves of NaYF₄:Tm³⁺(5%) unheated and heated for 30 minutes at 450 °C. Excitation and emission wavelengths were 471 nm and 642 nm, respectively. b) Emission spectrum of NaYF₄:Tm³⁺(5%)/NaGdF₄ NCs unheated and heated for 30 minutes at 350 °C. Excitation wavelength was 465 nm.

that the decay curve changes upon heating. The emission spectra of unheated versus heated $\text{NaYF}_4:\text{Tm}^{3+}(5\%)/\text{NaGdF}_4$ NCs are shown in Figure 4.9.b. After diffusion we only expect the ratio between the two levels involved in cross-relaxation to change. However, we see that the peaks completely disappear in favour of a broad emission band, so the thulium emission also changes in a way that cannot be ascribed to diffusion. Therefore there is a strong indication of processes taking place beside diffusion, a possible explanation is the oxidation of Tm^{3+} to Tm^{2+} . Ultimately, these Tm^{3+} -doped nanocrystals are not suitable for the study of ion diffusion by means of luminescence.

4.2 Diffusion model

Quantitative determination of the diffusion coefficient for a specific host-lattice-dopant-ion combination requires a model that simulates diffusion as a function of time and subsequently translates these concentration profiles to luminescence decay curves. We use Fick's second law of diffusion to calculate the ion distribution over time. For each concentration in the gradient, we use the shell model to calculate the corresponding decay curve and sum all these curves to obtain the total decay curve for the nanocrystal, which we can then fit to the experimental data.

4.2.1 Calculating the concentration profile

First, we model the ion concentration profile over time. As initial and boundary conditions we consider a spherical, doped core with radius r and concentration ϕ_{NC} and a spherical, undoped shell (Figure 4.10.a). Therefore, our model is only accurate for approximately spherical NCs. To simulate the undoped shell, we implement the boundary condition that no ions can diffuse beyond the core/shell radius d and initially, the ion concentration $\phi = 0$ between r and d . Diffusion of the dopant follows Fick's second law so that the ions in the core diffuse to the shell (Figure 4.10.b). In the limit of infinite diffusion time, this concentration gradient converges to a homogeneous distribution of ions throughout the particle (Figure 4.10.c).

Fick's second law of diffusion cannot be solved analytically for our initial conditions. In order to solve the equation numerically, we divide our particle into cubic voxels with 0.1 nm edges and consider our NC to have its centre at $x = y = z = 0$. We assign $\phi = \phi_{\text{NC}}$ for voxels with coordinates $x^2 + y^2 + z^2 < r^2$ and $\phi = 0$ everywhere else. To calculate the diffusion within the particle we use the following discretised form of Fick's second law of diffusion:[39]

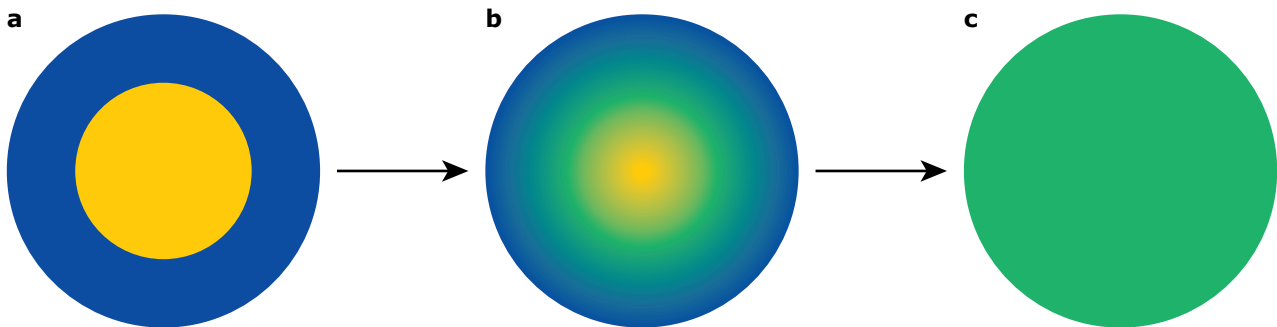


Figure 4.10: Schematic representation of the lanthanide-diffusion through a doped-core-undoped-shell nanocrystal.

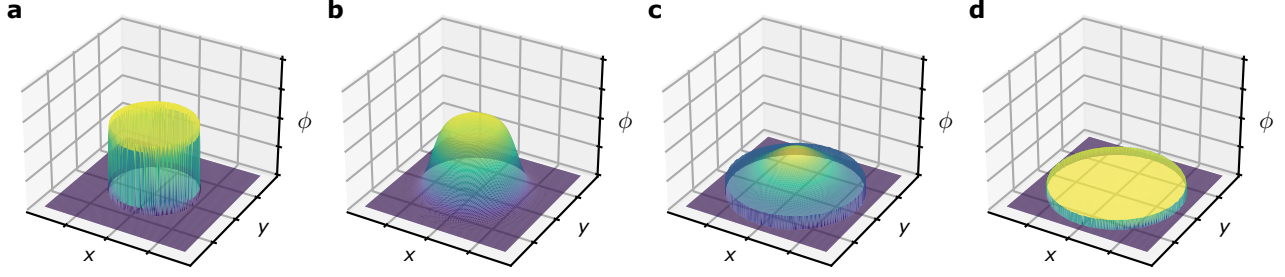


Figure 4.11: The dopant distribution over a cross section at $z = 0$ at a) $n = 0$, b) & c) intermittent time steps and d) the limit of n approaching infinity, where the dopants are distributed homogeneously over the entire NC.

$$\begin{aligned} \phi_{i,j}^{n+1} = & \phi_{i,j,k}^n + \frac{D\Delta t}{\Delta x^2}(\phi_{i+1,j,k}^n - 2\phi_{i,j,k}^n + \phi_{i-1,j,k}^n) + \frac{D\Delta t}{\Delta y^2}(\phi_{i,j+1,k}^n - 2\phi_{i,j,k}^n + \phi_{i,j-1,k}^n) \\ & + \frac{D\Delta t}{\Delta z^2}(\phi_{i,j,k+1}^n - 2\phi_{i,j,k}^n + \phi_{i,j,k-1}^n) \end{aligned} \quad (4.1)$$

where $\phi_{i,j,k}$ is the ion concentration in the voxel with coordinates i , j , and k , which are indexes that take all values of x , y , and z , respectively, keeping the total number of dopant ions in the NC constant over time. The superscript n denotes the number of time steps with length Δt . Δx , Δy , Δz are the step length in x , y , and z direction respectively. D is the diffusion coefficient. For our calculations, we used a constant

$$C = \frac{D\Delta t}{l^2} \quad (4.2)$$

to control the speed of diffusion in our model without having to know Δt and D a priori. l is the length of our voxel edges, which is the same step length in all three dimensions, so $l = \Delta x = \Delta y = \Delta z$. Figure 4.11 shows the ion concentration at different n as two dimensional diffusion profiles at $z = 0$. Panel a) shows the initial dopant distribution at $n = 0$, where we see a high dopant concentration in the core and $\phi = 0$ everywhere else. Panel d) is the distribution at large n after homogeneous distribution has been reached, so here we see the same, low concentration across the whole NC. Panel b) and c) are the concentration gradients at intermittent time steps, where we see an inhomogeneous distribution, with the highest dopant percentage in the centre and lower concentrations towards the edge of the NC. As we have successfully calculated the ion distribution over time, the next step is the translation into decay curves.

4.2.2 From concentration profile to decay curve

We use the shell model to translate the simulated ionic distribution (Section 4.2.1) to a decay curve. The shell model takes one value for the ion concentration as input (Section 2.3). However, as a result of diffusion there is a concentration gradient, as opposed to a single value across the entire particle. In this gradient, the ion concentration per voxel is known, as calculated by the diffusion model. Therefore, we can simply calculate the decay curve for each voxel and sum them to find the decay curve for the entire nanocrystal (Figure 4.12).

Figure 4.13 shows four examples of decay curves resulting from this calculation. The concentration gradients are also given in the respective colours. We show our initial condition in

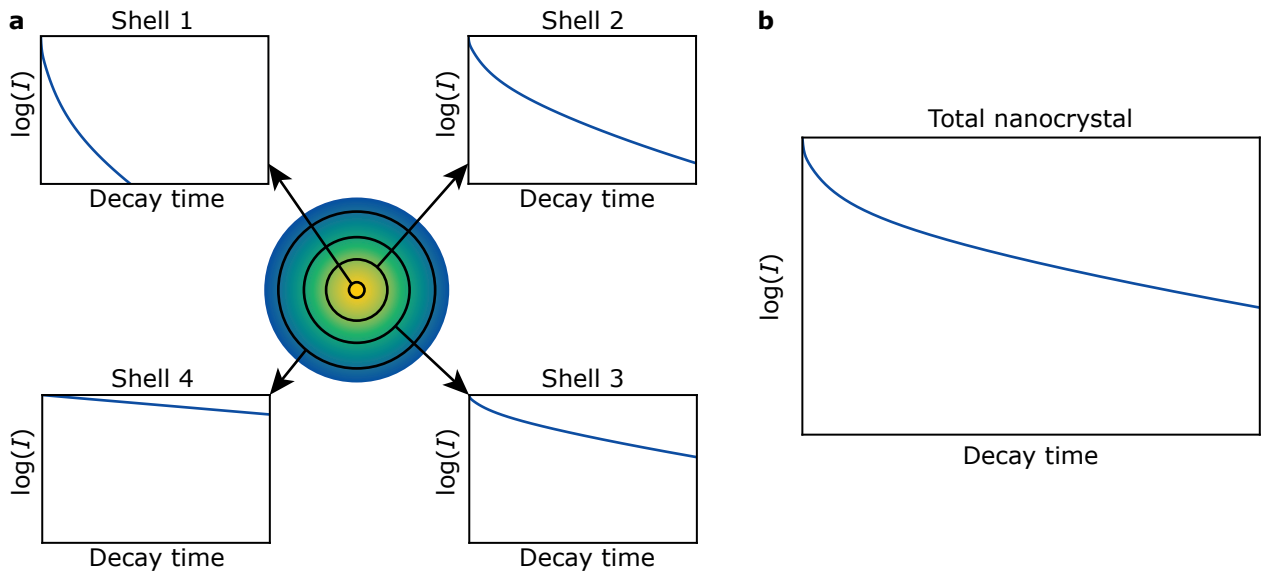


Figure 4.12: a) A schematic representation of a concentration gradient in a particle and the decay curves that correspond to ions at four different radial positions. b) The resulting decay curve from combining those in a).

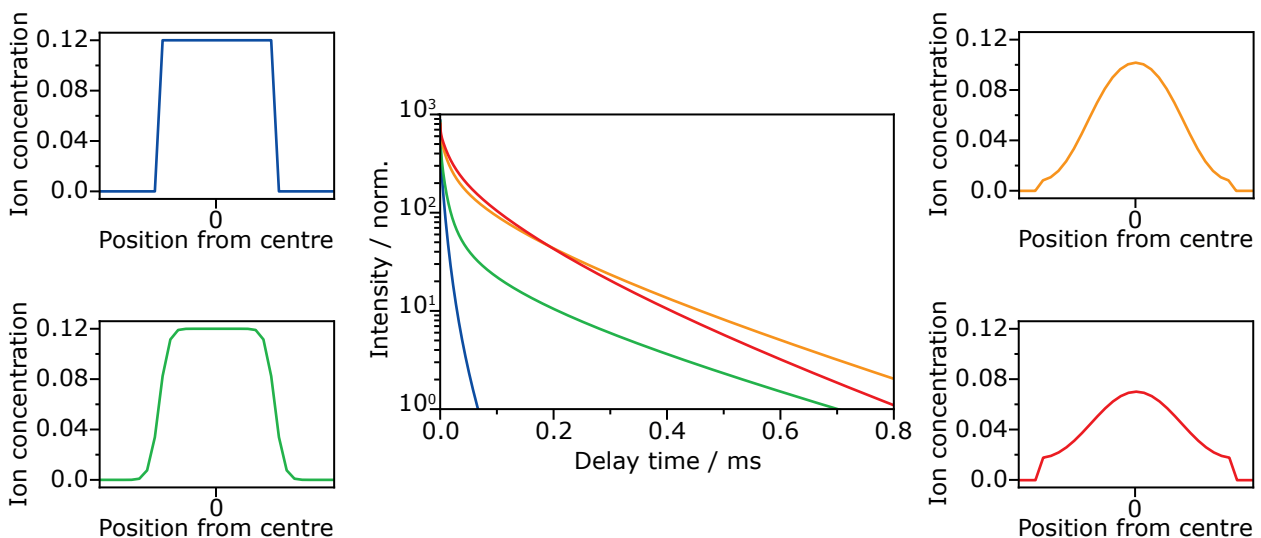


Figure 4.13: Four examples of concentration gradients and their respective decay curves.

blue, with ϕ_{NC} in the core and $\phi = 0$ elsewhere. As all the dopants experience a large number of neighbours, there is efficient cross-relaxation, resulting in fast decay. At longer diffusion times (green), we observe that there has been some diffusion, especially at the edge of the core. Consequently, there is still a high concentration in the core, which results in a fast decay at short delay times. However, there is also a fraction of ions a short distance from the core where the number of neighbours drops significantly. These luminescent centres have less efficient cross-relaxation as the distance between ions is relatively large. In the decay curve this is seen as a slow decaying tail at long delay times. After more diffusion, the slow decaying tail remains as there are still ions experiencing a low concentration. However, the concentration in the centre reduces, resulting in a significantly slower decay at short delay times (orange curve). With further diffusion the ions reach the edge of the particle and their concentration increases, resulting in a faster decay at longer delay times (red line). From Figure 4.13 we can

conclude that the model simulates decay curves that are in accordance with the trend expected for diffusion in a core/shell nanocrystal.

Finally, we want to determine the diffusion coefficient from our experimental decay curves. First, we calculate the concentration profiles and corresponding decay curves for a range of time steps n (Section 4.2.1), amplitudes I_0 , and background levels y_0 . Next, we fit calculated decay curves to the experimental decay curve measured from NCs heated for a time t . The best fit gives us the number of time steps required to reach the same concentration profile as the heated NCs. By dividing the actual heating time t by the number of time steps n , we calculate the length of the time steps Δt . We rewrite Equation 4.2 to

$$D = \frac{Cl^2}{\Delta t} \quad (4.3)$$

where we fill in the Δt calculated, our voxel length 0.1 nm as l and the value of C as used in our model (Section 4.13) to obtain the diffusion coefficient D of our system. We can use the diffusion coefficient to compare the diffusion speed for different temperatures and host lattice materials.

4.3 Model fit to experimental data

To determine the diffusion coefficient of holmium in NaYF₄/NaYF₄ and NaYF₄/NaGdF₄ core/shell NCs, we fit our diffusion model to the decay curves measured after different heating temperatures and times. We exclude terbium and thulium from this analysis, as we cannot qualitatively relate the experimental results to diffusion effects.

4.3.1 Diffusion during synthesis

We first discuss the diffusion of ions during the NC synthesis by comparing core and core/shell decay curves. Figure 4.14 shows the decay curves measured from NaYF₄:Ho³⁺(12%) core (panel a)) and NaYF₄:Ho³⁺(12%)/NaYF₄ (panel b) and c)) core/shell NCs. We fit the decay from the core-only NCs to the shell model for a homogeneous distribution of dopant ions with the

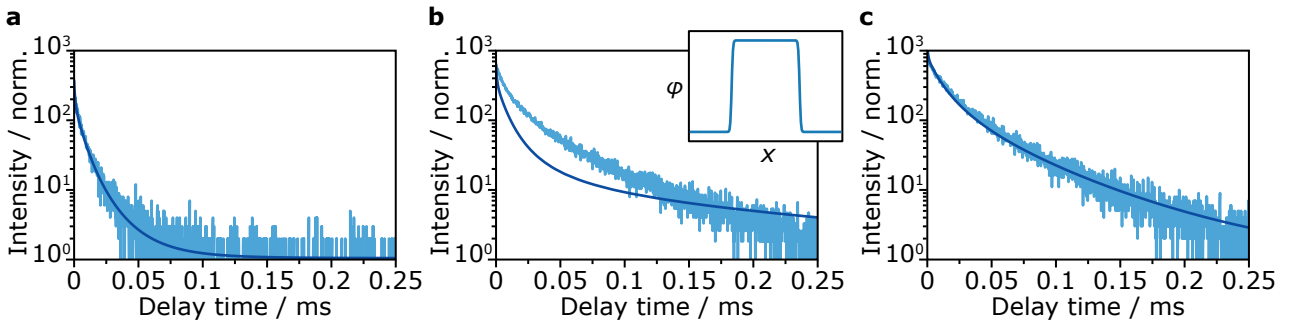


Figure 4.14: Luminescence decay curves of the ⁵S₂ emission (551 nm, excited by 532 nm light) of a) NaYF₄:Ho³⁺(12%) fit to the shell model for a homogeneous distribution of dopant ions, using ϕ , the amplitude I_0 and the background y_0 as fit parameters (best fit for $\phi = 0.12$) and b) NaYF₄:Ho³⁺(12%)/NaYF₄ fit to the diffusion model and corresponding diffusion gradient. c) Same as a) but with NaYF₄:Ho³⁺(12%)/NaYF₄ NCs and the best fit was achieved for $\phi = 0.06$.

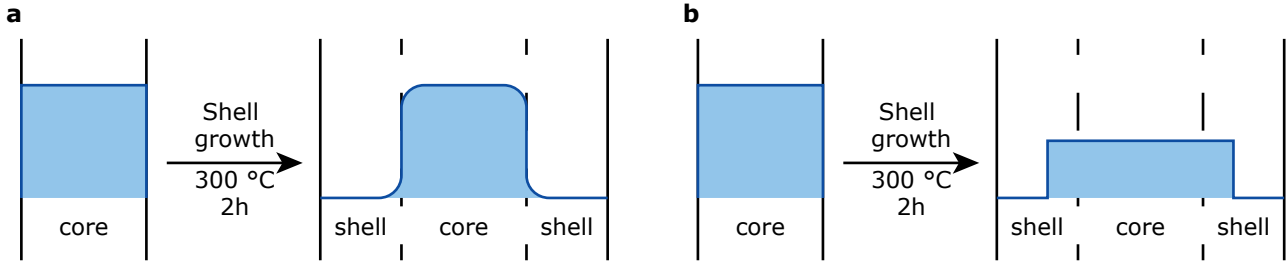


Figure 4.15: a) The ionic distribution after shell synthesis expected from literature.[35][36][37]. b) The ionic distribution after shell synthesis determined from model fits.

dopant concentration as fit parameter. The best fit was achieved with a 12% doping concentration, which is in agreement with the amount of holmium added during synthesis. To determine the extent of diffusion from the core to the shell during synthesis (Section 4.1.1), we fit decay curves calculated from a multitude of concentration profiles to the decay data of $\text{NaYF}_4:\text{Ho}^{3+}(12\%)/\text{NaYF}_4$ NCs. The best fit and corresponding concentration gradient are shown in Figure 4.14.b. Clearly, the model fits the experimental data poorly. To gain further insight into the ion distribution in the core/shell NCs, we fit the shell model for homogeneous ion distribution to the experimental decay curve (Figure 4.14.c). The fit agreed well for a dopant concentration of 6% holmium. This suggests that there is a complete restructuring of the core during shell synthesis, resulting in a larger core with lower concentration (Figure 4.15.b), in contrast to the expected low-scale diffusion of ions at the core/shell interface (Figure 4.15.a). Alternatively, the poor fit of the diffusion model might be caused by the assumption that cross-relaxation efficiency can be calculated from the concentration within a voxel, while cross-relaxation is actually effective on a scale larger than the voxel size.

4.3.2 Further diffusion during heating

To study the effect of heating on the distribution of lanthanides in our synthesised NCs, we use the size of these NCs as initial and boundary conditions for our model. We use the situation as depicted in Figure 4.15.b as our initial conditions for the calculation of the concentration profile after additional heating. To calculate the size of the enlarged core, we need the ratio between core and core/shell volume. As the total number of ions stays constant, the ratio between the unheated core concentration and the concentration in the entire core/shell NC after heating to homogeneous distribution gives the ratio between the core and core/shell volume. We determine the latter concentration by fitting the shell model to the decay curve of the core/shell NCs heated at 550 °C for 30 minutes. The best fit is achieved for an ion concentration of 1.6% (Appendix 6.3). With the known size of the core/shell NCs (Section 4.1.1) we calculate a core radius of 4.9 nm. Having determined the initial and boundary conditions corresponding to the NCs used for experimental work, we can calculate the concentration profiles of these NCs over time and their respective decay curves.

We fit the calculated decay curves to the experimental decay curves of $\text{NaYF}_4:\text{Ho}^{3+}/\text{NaYF}_4$ NCs heated for 10, 20, 30, and 60 minutes at 350 °C (Figure 4.16) to determine the diffusion coefficient for holmium in NaYF_4 at this temperature (Section 4.2.2). The values we found for D are $1.67 \cdot 10^{-25}$, $5.00 \cdot 10^{-25}$, $1.22 \cdot 10^{-24}$, and $3.33 \cdot 10^{-24}$ m^2/s respectively, averaging to $1.31 \cdot 10^{-24}$ m^2/s . Reported values of D are not available for NaYF_4 , so we compare $1.35 \cdot 10^{-22}$

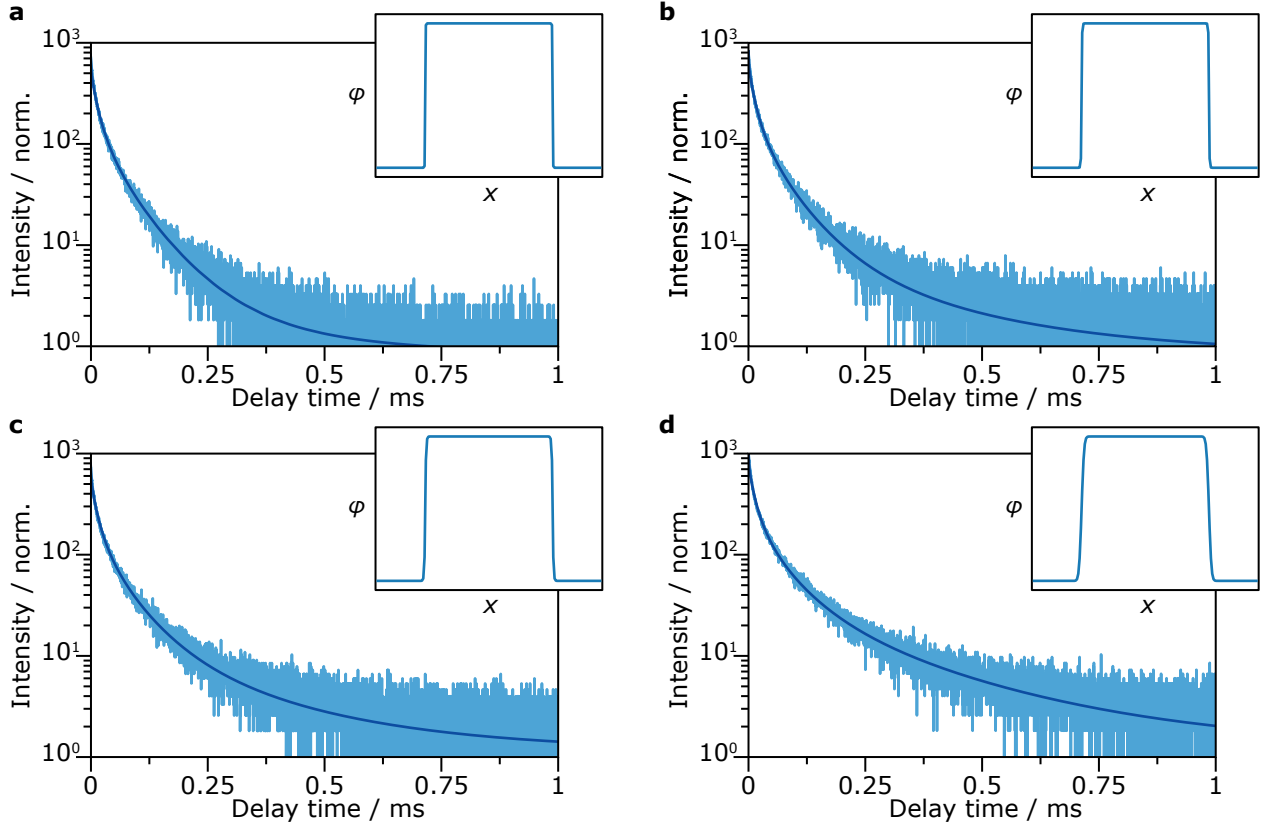


Figure 4.16: a) Luminescence decay curves of the 5S_2 emission (551 nm, excited by 532 nm light) of $\text{NaYF}_4:\text{Ho}^{3+}(12\%)/\text{NaYF}_4$ NCs heated for 10 minutes at 350 °C. Dark blue solid curve is the best fit of the diffusion model with corresponding concentration profile in the inset. b-d) same as a but heated for 20, 30, and 60 minutes, respectively.

for Dy^{3+} in YAG at 1150 °C to our results to conclude that our results are in a realistic order of magnitude.[23] Remarkably, there is an increasing trend with heating time while we expect the diffusion coefficient to be time independent. A possible cause is the additional diffusion during the warming up and cooling down of the sample that we did not account for in our calculations.

As we want to know the influence of temperature on diffusion speed, we use the same procedure to obtain the diffusion coefficient of $\text{NaYF}_4:\text{Ho}^{3+}(12\%)/\text{NaYF}_4$ NCs heated to 400 °C (Appendix 6.4). The diffusion coefficients from these experiments are $1.17 \cdot 10^{-22}$ (10 min), $9.92 \cdot 10^{-23}$ (20 min), $1.10 \cdot 10^{-22}$ (30 min), and $1.11 \cdot 10^{-22}$ (60 min) m^2/s , thus $1.11 \cdot 10^{-22}$ m^2/s on average. Most notably, the diffusion coefficient is two orders of magnitude higher at 400 °C than at 350 °C. The increase in D with temperature is in accordance with theory on diffusion (Section 2.4). As we only have diffusion coefficients for two temperatures we cannot conclude whether or not the increase follows Equation 2.8. Beside temperature, we also want to know the influence of the shell material on diffusion speed, therefore we heated $\text{NaYF}_4:\text{Ho}^{3+}(12\%)/\text{NaGdF}_4$ to 350 °C and 400 °C for the same time increments as used with $\text{NaYF}_4:\text{Ho}^{3+}(12\%)/\text{NaYF}_4$ (Appendix 6.5 & 6.6). At 350 °C we get the following diffusion coefficients: $2.17 \cdot 10^{-24}$, $5.83 \cdot 10^{-24}$, $7.78 \cdot 10^{-24}$, $8.06 \cdot 10^{-24}$ m^2/s for 10, 20, 30, and 60 minutes, respectively ($6.00 \cdot 10^{-24}$ m^2/s on average). In this same order, the coefficients are $1.02 \cdot 10^{-22}$, $1.22 \cdot 10^{-22}$, $1.20 \cdot 10^{-22}$, and $7.11 \cdot 10^{-23}$ m^2/s at 400 °C, averaging to $1.04 \cdot 10^{-22}$ m^2/s . These results are in line with those for the $\text{NaYF}_4:\text{Ho}^{3+}(12\%)/\text{NaYF}_4$ NCs. All diffusion coefficients are summarised in Figure 4.17. We have not found a significant difference between the diffusion coefficients of NCs with a NaYF_4

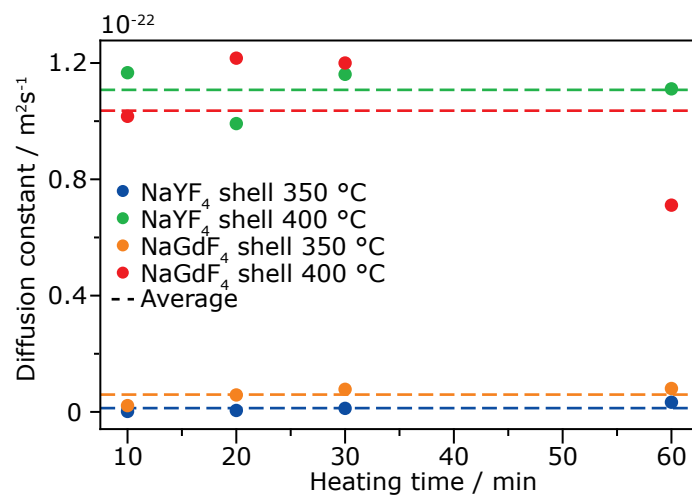


Figure 4.17: Diffusion coefficients of NaYF₄:Ho³⁺(12%)/NaYF₄ and NaYF₄:Ho³⁺(12%)/NaGdF₄ NCs heated at 350 °C and 400 °C for 10, 20, 30, and 60 minutes (circels) and the average over these four values (dashed line).

or NaGdF₄ shell when heated at the same temperature. While their values are not identical, the spread in the values of a single shell material and temperature suggest that the average value might not be accurate enough to establish any small differences for the two materials.

Chapter 5

Conclusion

We have developed a method to follow ion diffusion using luminescent decay curves. In this method, we model concentration profiles using Fick's second law of diffusion and translate these to decay curves. We test our model by comparing to experimental decay curves measured from core/shell nanocrystals (NCs) and found the model curves to be in accordance with experimental findings. We have successfully fit the experimental decay curves with the model to obtain the quantitative diffusion coefficients for the synthesised NCs. In order to assess the influence of temperature on diffusion, we heated $\text{NaYF}_4:\text{Ho}^{3+}/\text{NaYF}_4$ NCs to 350 °C and 400 °C. We found that the decay curves change more rapidly with heating time at higher temperatures. As decay rates depend on the local ion concentration, we conclude that ionic diffusion is faster at higher temperatures, which is confirmed by an increase in diffusion coefficient with temperature. Luminescent decay curves of $\text{NaYF}_4:\text{Ho}^{3+}/\text{NaGdF}_4$ NCs were found to be very similar to those of $\text{NaYF}_4:\text{Ho}^{3+}/\text{NaYF}_4$ NCs. As their average diffusion coefficients are very close together, we haven't reached a conclusion on the effect of shell material based on the quantitative data. The development of this method introduces a facile and quantitative technique to track ion diffusion in NCs, which can greatly help to evaluate the best synthesis methods and materials to make NCs with sharp core/shell interfaces. Furthermore, does this method open up the possibility of using core/shell NCs as thermal history sensors.

Chapter 6

Outlook

In order to expand our knowledge on ion diffusion in nanocrystals, there are a few aspects of our method that might be investigated more. Firstly, it would be interesting to further explore the row of lanthanides to find suitable dopant ions besides holmium. A requirement for lanthanides to be used in the study of ion distribution through luminescence is a cross-relaxation pathway. Therefore, promising lanthanides to use include praseodymium and neodymium, where (${}^3P_0, {}^3H_4$) \rightarrow (${}^1D_2, {}^3H_6$) and (${}^4F_{3/2}, {}^4I_{9/2}$) \rightarrow (${}^4I_{15/2}, {}^4I_{15/2}$) cross-relaxations occur, respectively. Expanding the experimental data with other temperatures and host materials would also be worthwhile. Furthermore, it would be a useful future endeavour to check the accuracy of the model by comparing the results to monte-carlo simulations.

By improving the accuracy of the diffusion model and the reliability of the experimental set-up (specifically heating), more exact values for the diffusion coefficients could be determined. Then, the temperature dependence of the diffusion coefficient for a specific dopant-ion-crystal lattice combination could be quantified by heating at more temperatures. These nanocrystals could then be used as thermal history sensors where the temperature can be determined after heating, as long as the heating duration is known. Further research into different lanthanide dopants and host crystals might lead to discovery of other materials suitable for the study of ion diffusion. If these systems have diverse diffusion coefficients and emission wavelengths to measure their decay curves separately, we could combine two of these materials and simultaneously heat them, providing us with two separate equations for two distinct diffusion coefficients, sharing the same heating time and temperature. We can solve this system of two equations for our two unknowns, temperature and time. In this way we could create a very reliable thermal history sensor that can measure the temperature, as well as the duration of a heating event independently and simultaneously.

Acknowledgements

First of all, I would like to thank Thomas for his daily supervision. From new techniques in the lab and alignment methods for the Ekspla, to problem shooting in Python and Illustrator artistry, I learned a lot of new skills over the past year thanks to your supervision. I would also like to thank you for the many, many trips to the TEM.

Next, I would like to thank Andries for the useful discussions. Your suggestions really helped form new ideas for the project and understanding our results. Freddy I also want to thank for his advice, especially working on the model your ideas were a great help.

Lastly, a big thanks to the whole CMI group for not only making my thesis educational, but also a lot of fun. Everyone's door was always open for asking questions or advice and I really appreciated that. My fellow master students I mostly want to thank for making my time at CMI enjoyable and for being my moral support when stuff didn't go according to plan. Thank you all!

Bibliography

- [1] W. Gao, J. Dong, Z. Wang, Z. Zhang, H. Zheng, *Mater. Res. Bull.* 2017, 91, 77
- [2] K. Uheda, N. Hirosaki, H. Yamamoto, *Phys. Stat. Sol.* 2006, 203, 2712
- [3] M. Zhao, H. Liao, L. Ning, Q. Zhang, Q. Liu, Zhiguo Xia, *Adv. Mater.* 2018, 30, 1802489
- [4] P. Li, Z. Wang, Z. Yang, Q. Guo, *J. Mater. Chem. C* 2014, 2, 7823
- [5] C. Shi, X. Shen, Y. Zhu, X. Li, Z. Pang, M. Ge, M. Abolhasani, *ACS Omega* 2020, 5, 32420
- [6] J.F. Suyver, A. Meijerink, *C2W* 2002, 98, 12
- [7] G.-S. Yi, G.-M. Chowa, *J. Mater. Chem.* 2005, 15, 4460
- [8] H. Mai, Y. Zhang, R. Si, Z. Yan, L. Sun, L. You, C. Yan, *J. Am. Chem. Soc.* 2006, 128, 6426.
- [9] S. Wua,¹ G. Hana, D. J. Millirona, S. Alonia, V. Altoea, D. V. Talapinb, B. E. Cohena, P. J. Schuck, *PNAS* 2009, 106, 10917
- [10] D. K. Chatterjee, A. J. Rufaihah, Y. Zhang, *Biomaterials* 2008, 29, 937
- [11] Q. Liu, Y. Sun, T. Yang, W. Feng, C. Li, F. Li, *J. Am. Chem. Soc.* 2011, 133, 43, 17122
- [12] S. Fischer, N. D. Bronstein, J. K. Swabeck, E. M. Chan, A. P. Alivisatos, *Nano Lett.* 2016, 16, 7241
- [13] C. Homann, L. Krukewitt, F. Frenzel, B. Grauel, C. Würth, U. Resch-Genger, M. Haase, *Angew. Chem. Int. Ed.* 2018, 57, 8765
- [14] Y.-F. Wang, G.-Y. Liu, L.-D. Sun, J.-W. Xiao, J.-C. Zhou, C.-H. Yan, *ACS Nano* 2013, 7, 7200
- [15] L. Liu, X. Li, Y. Fan, C. Wang, A. M. El-Toni, M. Saleh Alhoshan, D. Zhao, F. Zhang, *Chem. Mater.* 2019, 31, 5608
- [16] B. Chen, D. Peng, X. Chen, X. Qiao, X. Fan, F. Wang, *Angew. Chem., Int. Ed.*, 2015, 54, 12788
- [17] P. U. Bastian, S. Nacak, V. Roddatis, M. U. Kumke, *J. Phys. Chem. C* 2020, 124, 11229
- [18] E. Wimmer, W. Wolf, J. Sticht, P. Saxe, C. B. Geller, R. Najafabadi, G. A. Young, *Phys. Rev. B* 2018, 77, 134305

- [19] P. L. Rupesh, M. Arulprakasajothi, *Int. J. Ambient* 2020, 2162
- [20] V. Ramakrishna (1970). *Diffusion in Solids*, Springer
- [21] P. Shewmon (2016). *Diffusion in Solids*, Springer
- [22] H. Mehrer (2007). *Diffusion in Solids*, Springer
- [23] D.J. Cherniak, *Phys. Chem. Miner.* 1998, 26, 156
- [24] B. Chen, D. Peng, X. Chen, X. Qiao, X. Fan, F. Wang, *Angew. Chem. Int. Ed.* 2015, 54, 12788
- [25] M.H.V. Werts, *Sci. Prog* 2005, 88, 101
- [26] V.A.G. Rivera, F.A. Ferri, E. Magera Jr. (2012). *Plasmonics - Principles and Applications*, IntechOpen, p. 293
- [27] J.-C. G. Bünzli, *Coord. Chem. Rev.* 2015, 293, 19
- [28] X. Zhu, X. Wang, H. Zhang, F. Zhang, *Angew. Chem. Int. Ed.* 2022, e202209378
- [29] T. P. van Swieten, D. Yu, T. Yu, S. J. W. Vonk, M. Suta, Q. Zhang, A. Meijerink, F. T. Rabouw, *Adv. Optical Mater.* 2021, 9, 2001518
- [30] J. Philibert, *Diffu. Fundam.* (2005), 2, 1.1
- [31] E. C. Aifantis, *Acta Mech.* 1980, 37, 265
- [32] Seoul National University, Chapter 2 Fickian Diffusion, accessed 24 November 2022, <https://ocw.snu.ac.kr/sites/default/files/NOTE/3887.pdf>
- [33] B. Grauel, C. Würth, C. Homann, L. Krukewitt, E. Andresen, J. Roik, S. Recknagel, M. Haase, U. Resch-Genger, *Nano Res.* 2022, 15, 2362
- [34] R. G. Geitenbeek, P. T. Prins, W. Albrecht, A. van Blaaderen, B. M. Weckhuysen, A. Meijerink, *J. Phys. Chem. C* 2017, 121, 3503–3510.
- [35] D. Hudry, R. Popescu, D. Busko, M. Diaz-Lopez, M. Abeykoon, P. Bordet, D. Gerthsen, I. A. Howard, B. S. Richards, *J. Mater. Chem. C* 2019, 7, 1164
- [36] D. Hudry, D. Busko, R. Popescu, D. Gerthsen, A. M. M. Abeykoon, C. Kubel, T. Bergfeldt, B. S. Richards, *Chem. Mater.*, 2017, 29, 9238
- [37] S. Duhnen, M. Haase, *Chem. Mater.* 2015, 27, 8375
- [38] R. Shannon, *Acta Cryst.* 1976, A32, 751.
- [39] L. A. Barba, G. F. Forsyth 2017, 12 steps to Navier–Stokes, accessed 24 November 2022, https://nbviewer.org/github/barbagroup/CFDPython/blob/master/lessons/09_Step_7.ipynb

Appendices

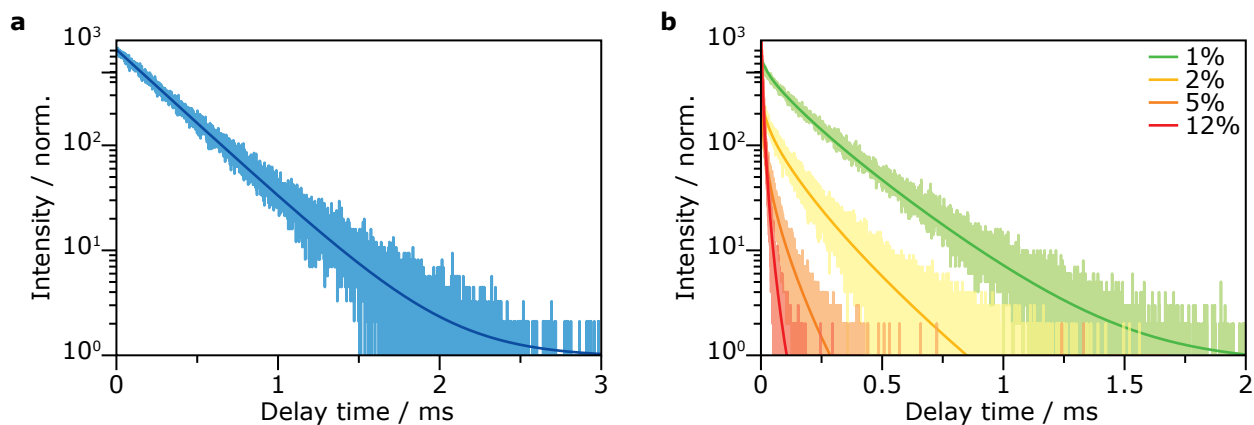


Figure 6.1: Luminescence decay curves of the 5S_2 emission of $\text{NaYF}_4:\text{Ho}^{3+}$ microcrystals. a) Crystals with 0.1% doping concentration fit with a mono-exponential function to find a k value of 3.0 ms^{-1} . b) Decay curves from crystals with 1%, 2%, 5%, and 12% holmium, fit with the shell model using C_X , the amplitude I_0 and the background y_0 as fit parameters to find a C_X value of $3.7 \cdot 10^6 \text{ \AA}^6/\text{ms}$. Excitation and emission wavelengths were 532 nm and 551 nm, respectively.

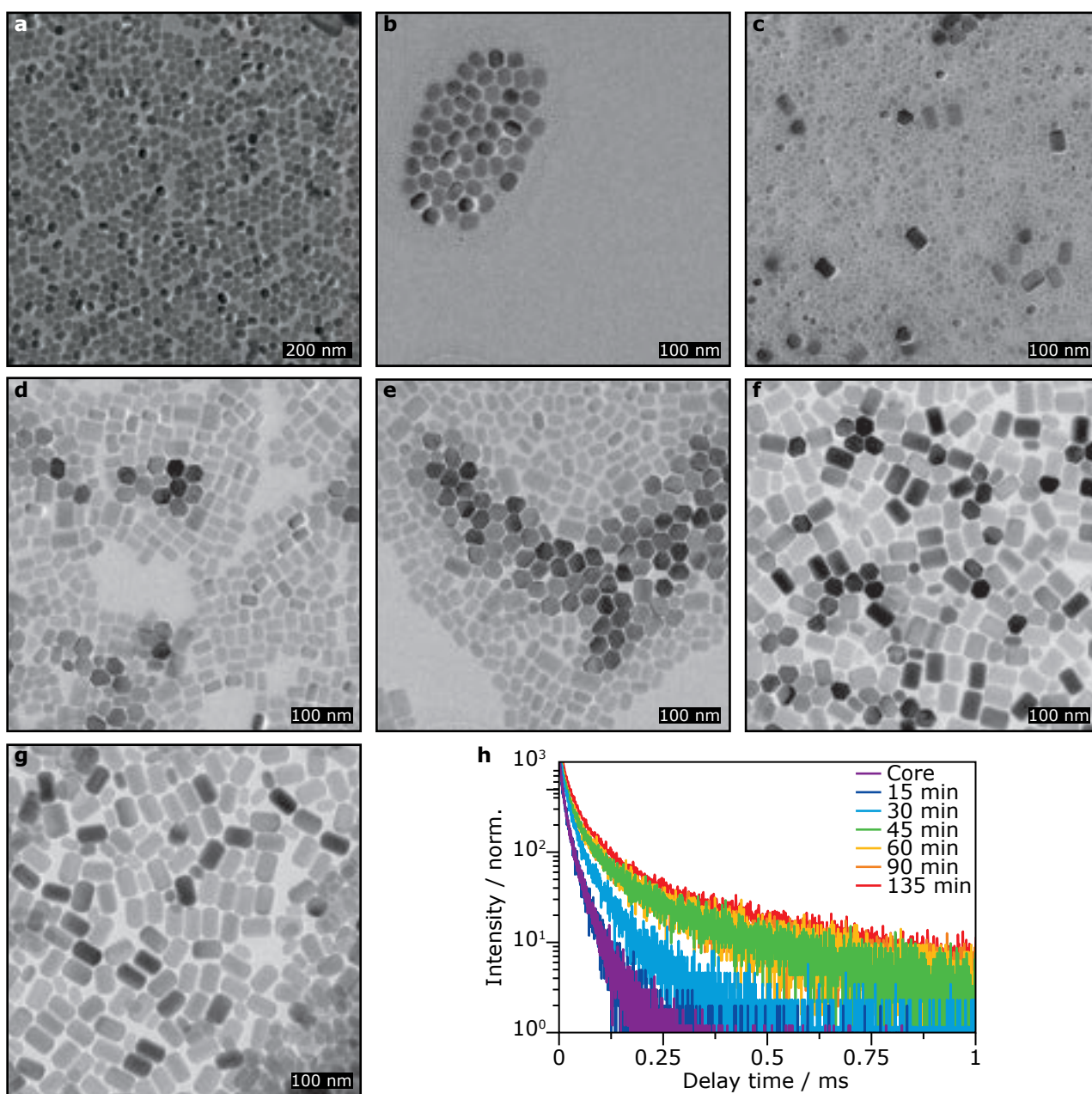


Figure 6.2: a) TEM image of NaYF₄:Ho³⁺(12%) NCs, synthesised using the method in Section 3.1.3. b) TEM image of intermittent product in the synthesis (Section 3.1.5) of a NaYF₄ shell around these cores after 15 minutes of heating the reaction mixture. c–f) Same as in b), but for heating times of 30, 45, 60 and 90 minutes, respectively. g) TEM image of the NaYF₄:Ho³⁺(12%)/NaYF₄ core/shell NCs after synthesis is completed (135 minutes). h) Luminescence decay curves of the NCs shown in a-g). Excitation and emission wavelengths were 532 nm and 551 nm, respectively.

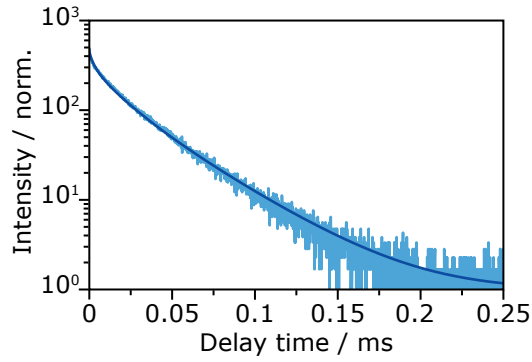


Figure 6.3: Luminescence decay curve of the 5S_2 emission (551 nm, excited by 532 nm light) of $\text{NaYF}_4:\text{Ho}^{3+}(12\%)/\text{NaYF}_4$ NCs heated for 60 minutes at 350 °C and 30 minutes at 550 °C, fit to the shell model for a homogeneous distribution of dopant ions, using ϕ , the amplitude I_0 and the background y_0 as fit parameters. Best fit for $\phi = 0.016$.

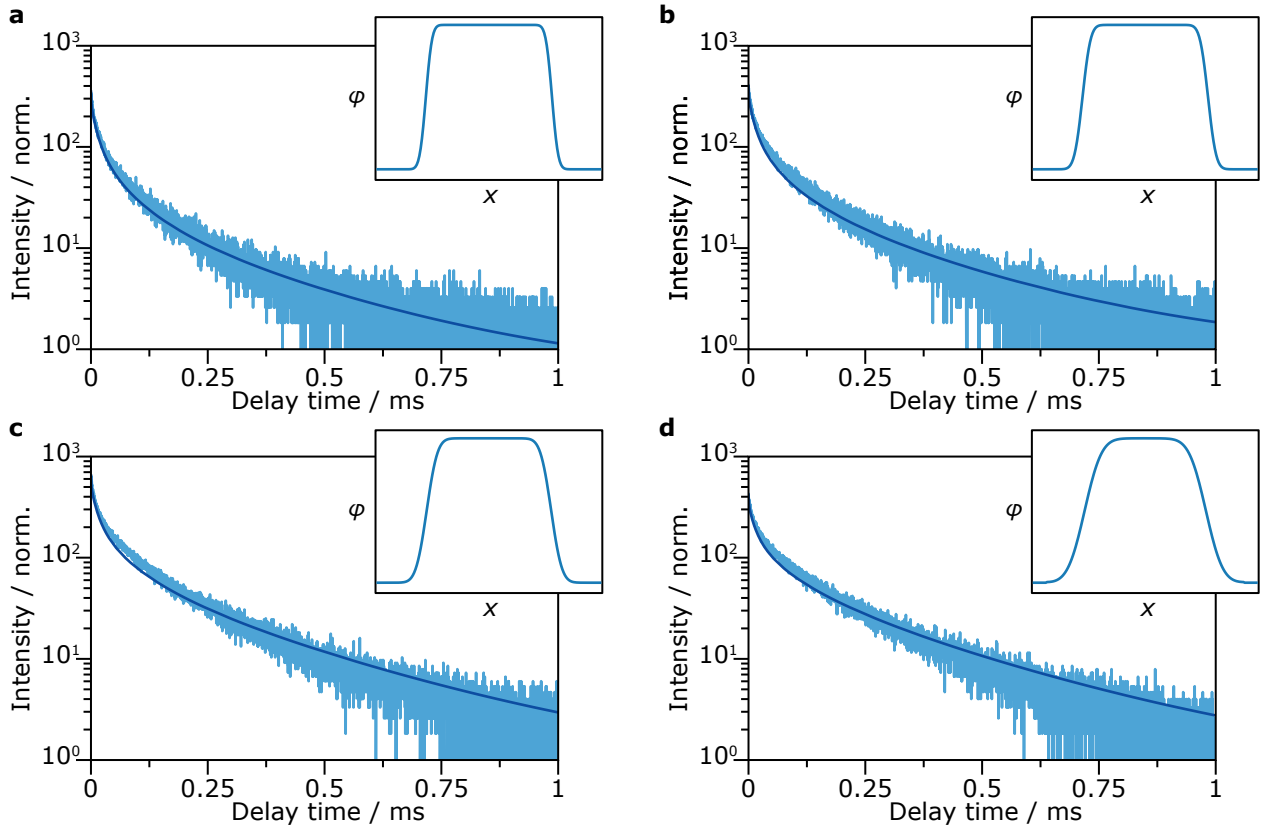


Figure 6.4: a) Luminescence decay curves of the 5S_2 emission (551 nm, excited by 532 nm light) of $\text{NaYF}_4:\text{Ho}^{3+}(12\%)/\text{NaYF}_4$ NCs heated for 10 minutes at 400 °C. Dark blue solid curve is the best fit of the diffusion model with corresponding concentration profile in the inset. b–d) Same as a) but heated for 20, 30, and 60 minutes, respectively.

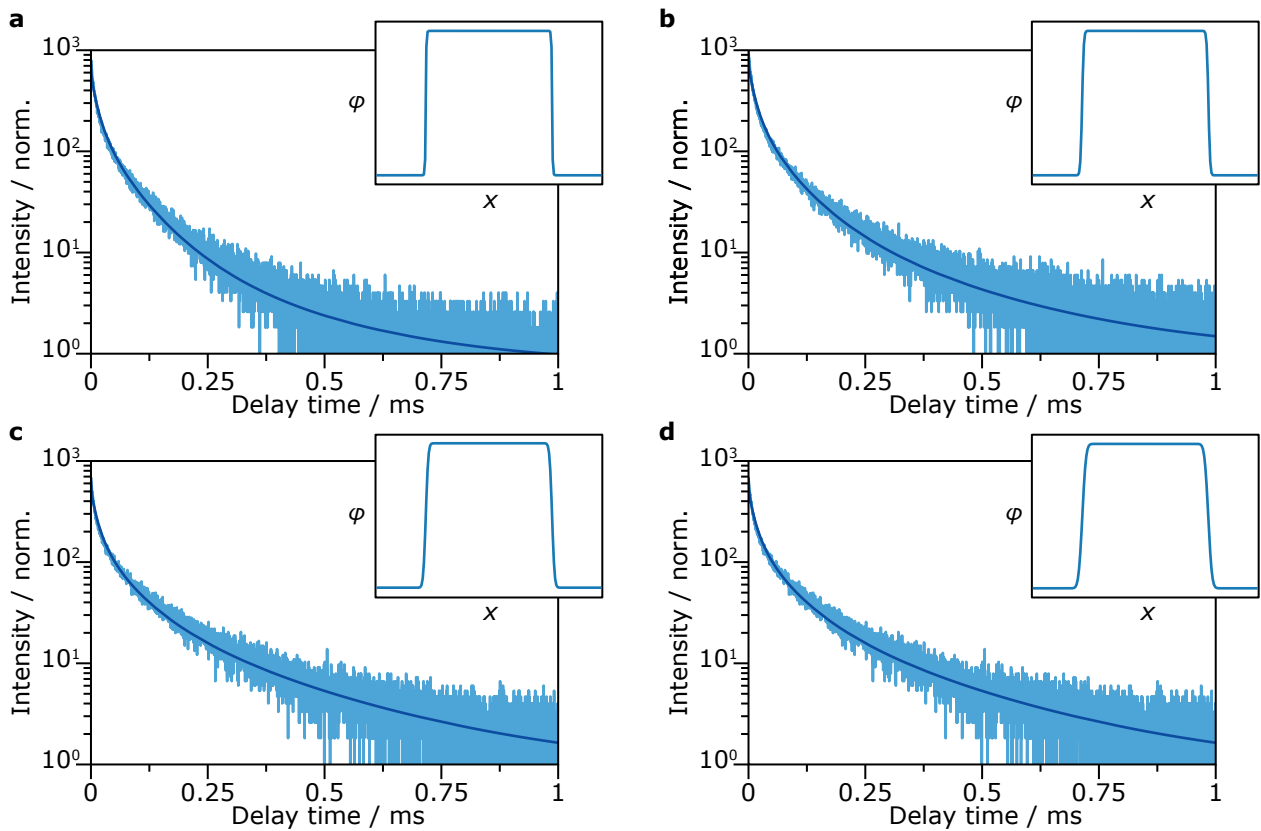


Figure 6.5: a) Luminescence decay curves of the 5S_2 emission (551 nm, excited by 532 nm light) of $\text{NaYF}_4:\text{Ho}^{3+}(12\%)/\text{NaGdF}_4$ NCs heated for 10 minutes at 350 °C. Dark blue solid curve is the best fit of the diffusion model with corresponding concentration profile in the inset. b–d) Same as a) but heated for 20, 30, and 60 minutes, respectively.

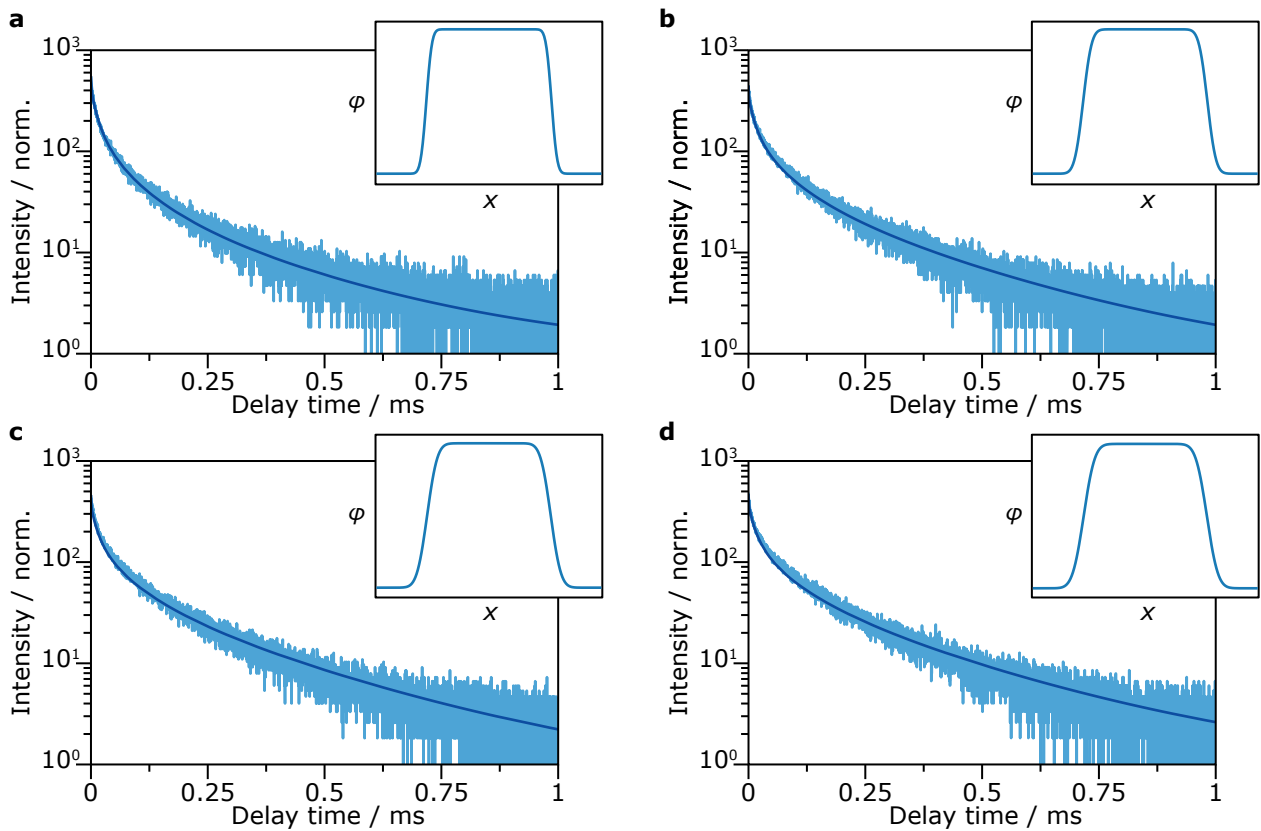


Figure 6.6: a) Luminescence decay curves of the 5S_2 emission (551 nm, excited by 532 nm light) of $\text{NaYF}_4:\text{Ho}^{3+}(12\%)/\text{NaGdF}_4$ NCs heated for 10 minutes at 400 °C. Dark blue solid curve is the best fit of the diffusion model with corresponding concentration profile in the inset. b–d) Same as a0 but heated for 20, 30 and, 60 minutes, respectively.